Effective Wavelet-Based Regularization of Divergence-free Fractional Brownian Motion

Patrick Héas, Souleymane Kadri Harouna, Pierre Dérian

EFFECTIVE WAVELET-BASED REGULARIZATION OF DIVERGENCE-FREE FRACTIONAL BROWNIAN MOTION

P. HÉAS*, S. KADRI-HAROUNA* AND P. DÉRIAN*

Abstract. This paper presents a method for regularization of inverse problems. The vectorial bi-dimensional unknown is assumed to be the realization of an isotropic divergence-free fractional Brownian Motion (fBm). The method is based on fractional Laplacian and divergence-free wavelet bases. The main advantage of these bases is to enable an easy formalization in a Bayesian framework of fBm priors, by simply sampling wavelet coefficients according to Gaussian white noise. Fractional Laplacians and the divergence-free projector can naturally be implemented in the Fourier domain. An interesting alternative is to remain in the spatial domain. This is achieved by the analytical computation of the connection coefficients of divergence-free fractional Laplacian wavelets, which enables to easily rotate this simple prior in any sufficiently "regular" wavelet basis. Taking advantage of the tensorial structure of a separable fractional wavelet basis approximation, isotropic regularization is then computed in the spatial domain by low-dimensional matrix products. The method is successfully applied to fractal image restoration and turbulent optic-flow estimation.

Key words. Bayesian modeling, fractional Brownian motion, divergence-free wavelets, fractional Laplacian, wavelet connection coefficients, fast recursive filtering, optic-flow, image restoration.

1. Introduction. Fractional Brownian motion (fBm) introduced by Mandelbrot and Van Ness [23] constitute popular models for the study of self-similar stochastic phenomena in a broad range of application domains such as statistical turbulence, network traffic analysis, financial markets or image processing. The practical interest of fBm models relies in their remarkable properties: Gaussianity, increments stationarity and statistical self-similarity. The latter property goes hand-in-hand with the empirical observation of inverse power-law power spectra in a wide range of applications, although the latter statement has to be made with caution as classical notion of power spectrum are not applicable for non-stationary signals [13]. Extensions of fBm have been proposed in the context of multidimensional signal analysis. In particular, there has been a special focus on the isotropic case [27], since isotropy constitutes a simple, yet relevant, assumption in numerous domain, including statistical turbulence [25]. Finally, vectorial fBm models first proposed in [25] have been recently studied systematically in [2, 30].

Interesting fBm decomposition can be designed by projection of fBm on wavelet bases. Indeed, non-stationarity and self-similarity of fBm necessitate some appropriate space-scale analysis brought by wavelet multiresolution analysis [14]. In particular, bi-orthogonal fractional wavelets constitute whitening filters for these signals, which are correlated both in space and scale [12, 24, 29, 30]. Moreover, in the context of turbulence studies, bi-orthogonal wavelet bases can also be designed to represent the space of divergence-free functions, which is a constraint of the incompressible Navier-Stokes equations [21]. Another advantageous property is the existence of a fast implementation of decomposition-reconstruction algorithms for those wavelets using recursive filter banks [1, 11].

FBm models have intensively been studied in the context of signal synthesis or analysis. In particular, many works deal with the synthesis of fBm (see *e.g.*, [1, 2, 14, 12, 24, 30]) or with the characterization of Hurst exponent from experimental data (see *e.g.*, [14, 6, 29]). However, suprinsingly, very little studies concern

*INRIA Rennes, Fluminance Team, Centre de Bretagne Atlantique, Université de Beaulieu, 35042 Rennes, France (Patrick.Heas@inria.fr)

Bayesian analysis and fBm models, *i.e.*, employing fBm prior models in inverse or ill-conditioned problems. The following works should nevertheless be mentioned, although they consider prior properties of fBm, and in particular an empirical power-law spectrum decay, rather than considering prior fBm models themselves. In the context of restoration of remote sensing imagery [18] or of magnetic resonance imaging [32], prior spectrum power-law decay have been used for the estimation of scalar fields from noisy or incomplete observations. Several recent works have also been led in this direction in the context of optic-flow estimation. In particular, prior power-law models for power spectra [10] or for structure functions [16] have recently been proposed in the context of turbulent motion estimation from image sequences.

This paper proposes a generic methodological framework for the regularization of ill-posed or ill-conditioned inverse problems using a bi-dimensional, and possibly divergence-free, fBm prior. The proposed model possesses a structure similar up to some extent to the regularizer proposed very recently in [31]. However, the modeling point of view adopted in this recent work is very different. Indeed, the authors do not intend to provide some prior model for fBm but rather propose regularization models satisfying invariance under coordinate transformations. Moreover, conversely to this related work, the present framework exploits an advantageous wavelet representation of fBm expressed in the spatial domain. Because of their advantageous whitening properties, divergence-free fractional Laplacian wavelet bases are chosen, yielding simple Gaussian white noise priors on wavelet coefficients. Furthermore, a low-complexity optimization algorithm, avoiding spectral computation and relying on mono-dimensional fast wavelet transforms, is proposed to maximize the posterior model.

The reminder of the paper is the following. After defining the properties of isotropic divergence-free fBm, we recall in the following section their spectral and wavelet representations. In section 3, we introduce a generic Bayesian framework for the regularization of inverse problems, based on the previous wavelet representation of fBm. Optimization algorithms for the maximization of the posterior model are then described in section 4. The modeling relevance and the algorithm efficiency are finally discussed in section 5, in the context of fractal image restoration and turbulent motion estimation.

2. Divergence-free isotropic fBm . For the clarity of the presentation, this work is restricted to the bi-dimensional case although it is in principle possible to extend the regularization to three dimensions. Moreover, in order to make the presentation as generic as possible, we focus on the more general case of divergence-free vectorial fields, keeping in mind that scalar fields or divergent vector fields are particular cases.

2.1. Divergence-free isotropic fBm definition and properties. The unique self-similar zero-mean Gaussian random process with stationary increments is fractional Brownian Motion (fBm) [13]. The definition of one-dimensional scalar fBm has been extended to the case of one-dimensional multivariate processes [2], to the case of isotropic -*i.e.*, multi-dimensional- scalar fields [27], or to the case of isotropic multivariate signals [25, 30]. We first recall the properties of the latter isotropic fBm model in the particular case of two-dimensional divergence-free vector fields.

Let $\boldsymbol{u}$ denote a realization[1] of the bi-dimensional divergence-free isotropic fBm random variable $\mathbf{u} = (\mathbf{u}_1, \mathbf{u}_2)^T$. Let us consider the Sobolev space of vectorial functions defined for $\zeta \in \mathbb{R}$ by:

$$(\mathcal{H}^\zeta(\mathbb{R}^2))^2 = \{\mathbf{f} \in (L^2(\mathbb{R}))^2 : (1-\Delta)^{\zeta/2}\mathbf{f} \in (L^2(\mathbb{R}^2))^2\}.$$

Realizations belong to the space of divergence-free functions:

$$\boldsymbol{u} = (\boldsymbol{u}_1, \boldsymbol{u}_2)^T \in \mathcal{H}^\zeta_{div}(\mathbb{R}^2) = \{\boldsymbol{u} \in \ (\mathcal{H}^\zeta(\mathbb{R}^2))^2 : \mathrm{div}_{\mathbf{x}}\boldsymbol{u} = 0\},$$

where the divergence operator is defined in the sense of distribution. More precisely, for any test function $\psi \in \mathcal{C}^1(\mathbb{R}^2)$ with a fast decay at infinity and with vanishing moments, we define the divergence operator by:

$$\begin{aligned} \mathrm{div}_{\mathbf{x}}\mathbf{u} &\triangleq \langle \mathrm{div}_{\mathbf{x}}\mathbf{u}, \psi\rangle_{L^2(\mathbb{R}^2)} \\ &= -\langle \mathbf{u}/\nabla_{\mathbf{x}}\psi\rangle, \end{aligned} \tag{2.1}$$

where $\langle .,. \rangle$ and $\langle ./. \rangle$ denote the inner product of two scalar (resp. two vectorial) functions in $L^2(\mathbb{R}^2)$ (resp. in $(L^2(\mathbb{R}^2))^2$). Definition (2.1) is necessary since fBm realizations are not continuously differentiable [13]. Divergence-free isotropic fBm are vectorial random fields in $\mathcal{H}^\zeta_{div}(\mathbb{R}^2)$ with the following properties [30]:

- zero-mean Gaussian variables,
- non-stationary vector fields with homogeneous increments,
- statistically invariant by rotation (isotropic),
- statistically self-similar with parameter $H \in [0,1]$.

Let us detail these properties. Statistical self-similarity and statistical rotation invariance are defined respectively by the following equality in probability law: for any orthogonal matrix M, *i.e.*, $MM^T = I$, $\forall \mathbf{x} \in \mathbb{R}^2$:

$$\mathbf{u}(\sigma\mathbf{x}) \overset{\mathcal{L}}{=} \sigma^H \mathbf{u}(\mathbf{x}),\ \forall \sigma \in \mathbb{R}+ \tag{2.2}$$

$$\mathbf{u}(\mathbf{x}) \overset{\mathcal{L}}{=} M\mathbf{u}(M^T\mathbf{x}), \tag{2.3}$$

where the real exponent H is known as the Hurst exponent.

The exponent has to be chosen as $H \in [0,1]$, since the Fourier integral defining the fBm process diverges for $H > 1$. Nevertheless, we will see that expanding fBm with wavelets with sufficiently vanishing moments enables the generalization to exponent $H \in \mathbb{R}_+/\mathbb{N}$ [6].

Non-stationarity of the random vector field $\mathbf{u}$ is a direct consequence of its self-similarity [13]. Let $\mathbb{E}_{\mathbf{u}}[\cdot]$ denote the expectation operator with respect to the probability distribution of $\mathbf{u}$. The isotropic divergence-free fBm increments are homogeneous and characterized by the following auto-correlation function [30]:

$$\begin{aligned} &\mathbb{E}_{\mathbf{u}}[(\mathbf{u}_i(\mathbf{x}+\boldsymbol{\tau}) - \mathbf{u}_i(\mathbf{x}-\mathbf{h}+\boldsymbol{\tau}))(\mathbf{u}_j(\mathbf{x}) - \mathbf{u}_j(\mathbf{x}-\mathbf{h}))^*] \propto \\ &\qquad [\mathbf{G}^H(\mathbf{h}+\boldsymbol{\tau})]_{ij} - 2[\mathbf{G}^H(\boldsymbol{\tau})]_{ij} + [\mathbf{G}^H(\mathbf{h}-\boldsymbol{\tau})]_{ij}, \qquad \forall H \in [0,1], \end{aligned} \tag{2.4}$$

with $\propto$ representing the symbol equal up to a multiplicative constant and where $[\mathbf{G}^H(\mathbf{h})]_{ij}$ is the (i,j)-th component of the 2 by 2 matrix $\mathbf{G}^H(\mathbf{h})$ defined by:

$$\mathbf{G}^H(\mathbf{h}) = \|\mathbf{h}\|^{2H}\left[\mathbf{I} - \frac{\mathbf{h}\mathbf{h}^T}{\|\mathbf{h}\|^2}\right]. \tag{2.5}$$

[1] Realizations of random variable are noted with calligraphic symbol. For example, a realization of the random variable $\mathbf{u}$ is noted $\boldsymbol{u}$.

The auto-correlation taken at $\boldsymbol{\tau}$=0 gives the second order moment of the increments:

$$\mathbb{E}_{\mathbf{u}}[(\mathbf{u}_i(\mathbf{x}) - \mathbf{u}_i(\mathbf{x}-\mathbf{h}))(\mathbf{u}_j(\mathbf{x}) - \mathbf{u}_j(\mathbf{x}-\mathbf{h}))^*] \propto [\mathbf{G}^H(\mathbf{h})]_{ij},\ \forall H \in [0,1], \tag{2.6}$$

For $H > 1$, one can show that the corresponding Gaussian fields have stationary increments of order $\lfloor H \rfloor + 1$ where $\lfloor H \rfloor$ denotes the largest integer lower or equal to H, see [30].

2.2. Spectral representation of fBm. Let $dW(\mathbf{k}) = (dW_1(\mathbf{k}), dW_2(\mathbf{k}))^T$ be the differential of a vectorial complex bi-dimensional Brownian motion satisfying the following properties:

$$dW_i(-\mathbf{k}) = dW_i^*(\mathbf{k}), \tag{2.7}$$
$$\mathbb{E}_W[dW_i(\mathbf{k})] = 0, \tag{2.8}$$
$$\mathbb{E}_W[dW_i(\mathbf{k})dW_j^*(\mathbf{k})] = \delta_{ij}d\mathbf{k}. \tag{2.9}$$

Isotropic divergence-free fBm components $\{\mathbf{u}_j | j = 1, 2\}$ can be equivalently defined in the Fourier domain by a Wiener integral.

PROPOSITION 2.1. *Any isotropic fBm* $\mathbf{u} \in \mathcal{H}^{\zeta}_{div}(\mathbb{R}^2)$ *of parameter* H *with* $\zeta = -H - 1$*, can be constructed by means of the spectral representation:*

$$\mathbf{u}(\mathbf{x}) - \mathbf{u}(0) = \frac{1}{(2\pi)^2}\int_{\mathbb{R}^2} \frac{(e^{i\mathbf{k}\cdot\mathbf{x}} - 1)}{\|\mathbf{k}\|}\sigma\mathbf{G}^{-\frac{H}{2}}(\mathbf{k})dW(\mathbf{k}) \tag{2.10}$$

where matrix $\mathbf{G}^{-\frac{H}{2}}$ *is given by* (2.5)*, where* σ *is a positive constant and* $dW(\mathbf{k})$ *is the differential of a vectorial complex bi-dimensional Brownian motion satisfying* (2.7)-(2.9).
That is to say, assuming a vanishing initial condition $\mathbf{u}_j(0) = 0$, the j-th component writes:

$$\mathbf{u}_j(\mathbf{x}) = \frac{1}{(2\pi)^2}\int_{\mathbb{R}^2} (e^{i\mathbf{k}\cdot\mathbf{x}} - 1)\sigma\|\mathbf{k}\|^{-H-1}\sum_i (\delta_{ij} - \frac{\mathbf{k}_i\mathbf{k}_j}{\|\mathbf{k}\|^2})dW_i(\mathbf{k}). \tag{2.11}$$

Proof. The construction of the fBm in the spectral domain is derived in an analogous manner as what has been done previously in the scalar isotropic case [27]. In order to be consistent with previous work [27, 30], we first define the frequency representation of an isotropic divergence-free fractional Gaussian noise by the Wiener integral:

$$\frac{1}{(2\pi)^2}\int_{\mathbb{R}^2} e^{i\mathbf{k}}\sigma\mathbf{G}^{-\frac{H}{2}}(\mathbf{k})dW(\mathbf{k}). \tag{2.12}$$

where the so-called fractal frequency filter $\mathbf{G}^{-\frac{H}{2}}(\mathbf{k})$ is given by (2.5). Then, using the fact that fBm increment between two position-vector points $\mathbf{x}$ and $\mathbf{y}$ is given by the integration of the fractional noise along the straight-line path, connecting $\mathbf{x}$ and $\mathbf{y}$ (see [27]) we obtain:

$$\mathbf{u}(\mathbf{x}) - \mathbf{u}(\mathbf{y}) = \frac{1}{(2\pi)^2}\int_{\mathbb{R}^2} \frac{(e^{i\mathbf{k}\cdot\mathbf{x}} - e^{i\mathbf{k}\cdot\mathbf{y}})}{\|\mathbf{k}\|}\mathbf{G}^{-\frac{H}{2}}(\mathbf{k})dW(\mathbf{k}). \tag{2.13}$$

□

2.3. Wavelet representations of fBm.

2.3.1. Motivations. The benefits of decomposing fBms on wavelet bases are listed below.

First, wavelets yield interesting fBm representations since non stationarity and self-similarity of fBm necessitate some appropriate space-scale analysis. Wavelets constitute whitening filters for these signals, which are correlated both in space and scale. The simplest choice is to use orthonormal wavelet bases. In this context, it can be shown that the variance of fBm wavelet coefficients decays through scales according to some power-law related to H [14]. Nevertheless, with orthonormal basis, coefficients remain correlated in space and scale, and only approximate fBm whitening filters can be designed. A better choice is to use bi-orthogonal fractional wavelet bases. They represent ideal whitening filters [12, 24, 29, 30]. Moreover, bi-orthogonal wavelet bases can also be designed to represent the space of divergence-free functions, which is a constraint of incompressible flows [21].

Second, choosing wavelets to expand fBm removes the singularity at the zero frequency in (2.11) for any Hurst exponent $H > 1$ as long as we are considering wavelets with sufficient vanishing moments [30]. Convergence of the Fourier integral is therefore guaranteed, and the concept of fBm may be extended to "integrated" forms.

The third argument is related to the special context of optimization in Bayesian analysis: wavelet multiresolution analyses of unknowns proved experimentally to be relevant optimization strategy for non-convex inverse problems [9]. Moreover, optimization can be led with a low-complexity since divergence-free wavelet decomposition [11] or the one-dimensional fractional wavelet decomposition [1] have an advantageous fast implementation with recursive filter banks [22].

We postpone the latter point to section 4 and introduce in the following representations of isotropic bi-dimensional fBm with divergence-free and fractional Laplacian wavelets.

2.3.2. Construction with divergence-free wavelets. To take into account implicitly the incompressibility constraint, the vectorial fBm $\mathbf{u}$ is represented in terms of divergence-free wavelet series [11]. The anisotropic[2] divergence-free wavelet spaces can be defined by:

$$\mathcal{H}^{\zeta}_{div}(\mathbb{R}^2) = \text{span}\{\Psi_{\boldsymbol{\ell},\mathbf{s}};\ \boldsymbol{\ell},\ \mathbf{s} \in\ \mathbb{Z}^2\} \tag{2.14}$$

with:

$$\Psi_{\boldsymbol{\ell},\mathbf{s}} = a_{\mathbf{s}}\mathbf{curl}[\chi_{\boldsymbol{\ell},\mathbf{s}}] \tag{2.15}$$

where $\mathbf{curl} \triangleq (\frac{\partial}{\partial \mathbf{x}_2}, -\frac{\partial}{\partial \mathbf{x}_1})^t$, $a_{\mathbf{s}} \triangleq \frac{1}{\sqrt{4^{s_1}+4^{s_2}}}$ and $\chi_{\boldsymbol{\ell},\mathbf{s}} = \psi_{\ell_1,s_1} \otimes \psi_{\ell_2,s_2}$ represents an orthonormal scalar basis of $L^2(\mathbb{R}^2)$, constructed using regular wavelets $\{\psi_{\ell,s} = 2^{s/2}\psi(2^s x - \ell); \ell, s \in \mathbb{Z}\}$. Wavelets[3] $\Psi_{\boldsymbol{\ell},\mathbf{s}}$ compose a primal vectorial basis of $(L^2(\mathbb{R}^2))^2$. Precisely, this primal divergence-free basis is constituted by wavelets $\Psi_{\boldsymbol{\ell},\mathbf{s}} = (\Psi^1_{\boldsymbol{\ell},\mathbf{s}}, \Psi^2_{\boldsymbol{\ell},\mathbf{s}})^T$, where $\Psi^1_{\boldsymbol{\ell},\mathbf{s}} = a_{\mathbf{s}}(\psi_{\ell_1,s_1} \otimes \frac{\partial}{\partial \mathbf{x}_2}\psi_{\ell_2,s_2})$ and $\Psi^2_{\boldsymbol{\ell},\mathbf{s}} = -a_{\mathbf{s}}(\frac{\partial}{\partial \mathbf{x}_1}\psi_{\ell_1,s_1} \otimes \psi_{\ell_2,s_2})$. Let us now consider measurements test functions constituted by the dual wavelets[4] $\tilde{\Psi}_{\boldsymbol{\ell},\mathbf{s}} = (\tilde{\Psi}^1_{\boldsymbol{\ell},\mathbf{s}}, \tilde{\Psi}^2_{\boldsymbol{\ell},\mathbf{s}})^T$, which are biorthogonal to the primal wavelets $\Psi_{\boldsymbol{\ell},\mathbf{s}}$. Using such test

[2] The anisotropy of the wavelet basis has not to be confused with the isotropy of the fBm model.

[3] with the L^2 norm $\|\Psi_{\boldsymbol{\ell},\mathbf{s}}\|^2 = \int_{\mathbb{R}^2} \sum_i \Psi^i_{\boldsymbol{\ell},\mathbf{s}}\Psi^i_{\boldsymbol{\ell},\mathbf{s}}(\mathbf{x})d\mathbf{x} = 1$

[4] with the L^2 norm $\|\tilde{\Psi}_{\boldsymbol{\ell},\mathbf{s}}\|^2 = \int_{\mathbb{R}^2} \sum_i \tilde{\Psi}^i_{\boldsymbol{\ell},\mathbf{s}}\tilde{\Psi}^i_{\boldsymbol{\ell},\mathbf{s}}(\mathbf{x})d\mathbf{x} = 1$

functions, one can decompose uniquely any divergence-free vector field $\mathbf{u} \in \mathcal{H}^{\zeta}_{div}(\mathbb{R}^2)$:

$$\mathbf{u} = \sum_{\boldsymbol{\ell},\ \mathbf{s}\ \in\ \mathrm{Z}^2} \langle \mathbf{u}/\tilde{\Psi}_{\boldsymbol{\ell},\mathbf{s}} \rangle \Psi_{\boldsymbol{\ell},\mathbf{s}}(\mathbf{x}). \tag{2.16}$$

Given this biorthogonal wavelet basis, the Wiener integral can be decomposed as an infinite sum of weighted independent standard Gaussian random variables, yielding the following result.

PROPOSITION 2.2. *Let $\mathbf{u} \in \mathcal{H}^{\zeta}_{div}(\mathbb{R}^2)$ be an isotropic fBm of parameter H, with ζ=-H-1 and let $\hat{\Psi}_{\boldsymbol{\ell},\mathbf{s}}$ be the Fourier transform of $\Psi_{\boldsymbol{\ell},\mathbf{s}}$. fBm $\mathbf{u}$ can be constructed by means of the divergence-free wavelet series:*

$$\mathbf{u}(\mathbf{x}) = c \sum_{\boldsymbol{\ell},\mathbf{s}} \epsilon_{\boldsymbol{\ell},\mathbf{s}} \int_{\mathbb{R}^2} (e^{i\mathbf{k}\cdot\mathbf{x}} - 1) \|\mathbf{k}\|^{\zeta} \hat{\Psi}_{\boldsymbol{\ell},\mathbf{s}}(\mathbf{k}) d\mathbf{k} \tag{2.17}$$

where $c = \sigma/(2\pi)^2$ is a positive constant and where the set of coefficients $\{\epsilon_{\boldsymbol{\ell},\mathbf{s}}, (\boldsymbol{\ell},\mathbf{s}) \in \mathbb{Z}^2\}$ are distributed according to independent and identically distributed (i.i.d) zero-mean Gaussians of variance equal to the L^2 norm of the dual wavelets, i.e., *$\epsilon_{\boldsymbol{\ell},\mathbf{s}} \sim \mathcal{N}(0, \|\tilde{\Psi}_{\boldsymbol{\ell},\mathbf{s}}\|^2)$.*

Proof. For any vectorial function $\mathbf{v} = (\mathbf{v}_1, \mathbf{v}_2)^t \in \mathrm{span}\{\tilde{\Psi}_{\boldsymbol{\ell},\mathbf{s}};\ \boldsymbol{\ell},\ \mathbf{s} \in\ \mathbb{Z}^2\}$, since the wavelets $\tilde{\Psi}_{\boldsymbol{\ell},\mathbf{s}}$ form a basis of this functional space, we have:

$$\int_{\mathbb{R}^2} \sum_i \hat{\mathbf{v}}_i(\mathbf{k}) dW_i(\mathbf{k}) = \int_{\mathbb{R}^2} \sum_{\ell,\mathbf{s},i} \langle \hat{\mathbf{v}}/\hat{\Psi}_{\boldsymbol{\ell},\mathbf{s}} \rangle \hat{\tilde{\Psi}}^i_{\boldsymbol{\ell},\mathbf{s}}(\mathbf{k}) dW_i(\mathbf{k}) = \sum_{\ell,\mathbf{s}} \langle \hat{\mathbf{v}}/\hat{\Psi}_{\boldsymbol{\ell},\mathbf{s}} \rangle \epsilon_{\boldsymbol{\ell},\mathbf{s}} \tag{2.18}$$

with

$$\epsilon_{\boldsymbol{\ell},\mathbf{s}} = \sum_i \int_{\mathbb{R}^2} \hat{\tilde{\Psi}}^{i*}_{\boldsymbol{\ell},\mathbf{s}}(\mathbf{k}) dW_i(\mathbf{k}), \tag{2.19}$$

where $\hat{\tilde{\Psi}}_{\boldsymbol{\ell},\mathbf{s}}$ is the Fourier transform of $\tilde{\Psi}_{\boldsymbol{\ell},\mathbf{s}}$. This equality stands for any test function $\mathbf{v}$. Therefore one obtains that the differential of Brownian motion can be decomposed as:

$$\sum_i dW_i(\mathbf{k}) = \sum_{\ell,\mathbf{s},i} \epsilon_{\boldsymbol{\ell},\mathbf{s}} \hat{\Psi}^i_{\boldsymbol{\ell},\mathbf{s}}(\mathbf{k}) d\mathbf{k}. \tag{2.20}$$

Since the L^2 norm is conserved in the Fourier domain because of Plancherel's theorem, by definition of the Wiener integral (2.19) we get:

$$\epsilon_{\boldsymbol{\ell},\mathbf{s}} \sim \mathcal{N}(0, \|\tilde{\Psi}_{\boldsymbol{\ell},\mathbf{s}}\|^2). \tag{2.21}$$

Thus, using (2.16), (2.11) can be rewritten as:

$$\mathbf{u}_j(\mathbf{x}) = \frac{1}{(2\pi)^2} \sum_{\boldsymbol{\ell},\mathbf{s},i} \epsilon_{\boldsymbol{\ell},\mathbf{s}} \int_{\mathbb{R}^2} (e^{i\mathbf{k}\cdot\mathbf{x}} - 1) \sigma \|\mathbf{k}\|^{-H-1} \left(\delta_{ji} - \frac{\mathbf{k}_j \mathbf{k}_i}{\|\mathbf{k}\|^{\mathbf{2}}} \right) \hat{\Psi}^i_{\boldsymbol{\ell},\mathbf{s}}(\mathbf{k}) d\mathbf{k}. \tag{2.22}$$

The term $(\delta_{ji} - \frac{\mathbf{k}_j \mathbf{k}_i}{\|\mathbf{k}\|^{\mathbf{2}}})$ represents the symbol of Leray orthogonal projector, from $(L^2(\mathbb{R}^2))^2$ to the divergence-free function space $\mathcal{H}^{\zeta}_{div}(\mathbb{R}^2)$. Since divergence-free wavelets satisfy by construction

$$\sum_i \epsilon_{\boldsymbol{\ell},\mathbf{s}} (\delta_{ji} - \frac{\mathbf{k}_j \mathbf{k}_i}{\|\mathbf{k}\|^{\mathbf{2}}}) \hat{\Psi}^i_{\boldsymbol{\ell},\mathbf{s}} = \epsilon_{\boldsymbol{\ell},\mathbf{s}} \hat{\Psi}^j_{\boldsymbol{\ell},\mathbf{s}},$$

this operator can be removed, yielding the divergence-free wavelet representation of isotropic fBm (2.17).

□

From proposition 2.2, we can derive the structure of the expected isotropic power spectrum, which is in agreement with [27].

COROLLARY 2.1. *Let $\mathcal{S}(\kappa)$ represent the sphere around wave number κ. The mean expected two-dimensional power spectrum of $\mathbf{u} \in \mathcal{H}^{\zeta}_{div}(\mathbb{R}^2)$, with ζ=-H-1 obeys to the following power-law:*

$$\begin{aligned} E_{2d}(\kappa) &\triangleq \frac{1}{2\pi\|\mathbf{k}\|}\int_{\mathcal{S}(\kappa=\|\mathbf{k}\|)} \mathbb{E}_{\epsilon_{\boldsymbol{\ell},\mathbf{s}}}[\|c\sum_{\boldsymbol{\ell},\mathbf{s}} \epsilon_{\boldsymbol{\ell},\mathbf{s}}\|\mathbf{k}\|^{-H-1}\hat{\Psi}_{\boldsymbol{\ell},\mathbf{s}}(\mathbf{k})\|^2]d\mathbf{k} \\ &= c^2\sum_{\boldsymbol{\ell},\mathbf{s}} \mathbb{E}_{\epsilon_{\boldsymbol{\ell},\mathbf{s}}}[\|\epsilon_{\boldsymbol{\ell},\mathbf{s}}\|^2]\|\mathbf{k}\|^{-2H-2} \propto \kappa^{-2H-2}, \end{aligned} \tag{2.23}$$

resulting in the following expected isotropic power spectrum,

$$E(\kappa) \triangleq 2\pi\kappa E_{2d}(\kappa) \propto \kappa^{-2H-1}$$

When mentioned in the following, we may consider an isotropic power spectrum decay κ^{-2H-1} occurring on a bounded spectral interval $\Upsilon \subset \mathbb{R}$.

2.3.3. Construction with fractional Laplacian wavelets. The term $\|\mathbf{k}\|^{\zeta}\hat{\Psi}^j_{\boldsymbol{\ell},\mathbf{s}}(\mathbf{k})$ in (2.17) represents in the Fourier domain the wavelet fractional Laplacian $(-\Delta)^{\frac{\zeta}{2}}\Psi^j_{\boldsymbol{\ell},\mathbf{s}}(\mathbf{x})$. Thus, (2.17) can be rewritten as a linear combination of fractional Laplacian wavelets, yielding a divergence-free fractional Laplacian representation:

$$\mathbf{u}_j(\mathbf{x}) = c\sum_{\boldsymbol{\ell},\mathbf{s}} \epsilon_{\boldsymbol{\ell},\mathbf{s}}(-\Delta)^{\frac{\zeta}{2}}\left(\Psi^j_{\boldsymbol{\ell},\mathbf{s}}(\mathbf{x}) - \Psi^j_{\boldsymbol{\ell},\mathbf{s}}(\mathbf{x})\Big|_{\mathbf{x}=0}\right). \tag{2.24}$$

Indeed, one can define the fractional differentiation operator D^{ζ} in the Fourier domain by [24]:

$$\hat{D}^{\zeta} = (ik)^{\zeta} \tag{2.25}$$

and thus obtain the divergence fractional wavelets:

$$\widehat{(-\Delta)^{\frac{\zeta}{2}}\Psi^j_{\boldsymbol{\ell},\mathbf{s}}}(\mathbf{k}) = (-(i\|\mathbf{k}\|)^2)^{\frac{\zeta}{2}}\hat{\Psi}^j_{\boldsymbol{\ell},\mathbf{s}}(\mathbf{k}) = \|\mathbf{k}\|^{\zeta}\hat{\Psi}^j_{\boldsymbol{\ell},\mathbf{s}}(\mathbf{k}), \tag{2.26}$$

where $(\Delta)^{\zeta} = (D_x^2 + D_y^2)^{\zeta}$ represents a fractional Laplacian differentation. Note that the fractional differentiation preserves the divergence-free property:

$$\mathbf{k}\cdot\widehat{(-\Delta)^{\frac{\zeta}{2}}\Psi}_{\boldsymbol{\ell},\mathbf{s}}(\mathbf{k}) = \mathbf{k}\cdot\|\mathbf{k}\|^{\zeta}\hat{\Psi}_{\boldsymbol{\ell},\mathbf{s}}(\mathbf{k}) = \|\mathbf{k}\|^{\zeta}\mathbf{k}\cdot\hat{\Psi}_{\boldsymbol{\ell},\mathbf{s}}(\mathbf{k}) = 0, \tag{2.27}$$

with the notation $(-\Delta)^{\frac{\zeta}{2}}\Psi_{\boldsymbol{\ell},\mathbf{s}} = a_{\mathbf{s}}\mathbf{curl}[(-\Delta)^{\frac{\zeta}{2}}\chi_{\boldsymbol{\ell},\mathbf{s}}]$.

Let us now introduce bi-dimensional vectorial functions of $\mathcal{H}^{\zeta}_{div}(\mathbb{R}^2)$: $\Phi_{\boldsymbol{\ell},s_i} = (\Phi^1_{\boldsymbol{\ell},s_i}, \Phi^2_{\boldsymbol{\ell},s_i})^T = \frac{1}{\sqrt{2}}\mathbf{curl}[\chi^0_{\boldsymbol{\ell},s_i}]$ with $\chi^0_{\boldsymbol{\ell},s_1} = \psi_{\ell_1,s_1}\otimes\varphi_{\ell_2,0}$ and $\chi^0_{\boldsymbol{\ell},s_2} = \varphi_{\ell_1,0}\otimes\psi_{\ell_2,s_2}$, where $\varphi_{\ell,0}$ denote scaling functions at scale $2^{-0}=1$ associated to the scalar orthonomal wavelets $\psi_{\ell,\mathbf{s}}$. According to the work of Meyer [24], the low frequency contribution

in the fBm representation of (2.24) can be isolated, yielding the following corollary to proposition 2.2:

COROLLARY 2.2. *Let* $\mathbf{u} \in \mathcal{H}^{\zeta}_{div}(\mathbb{R}^2)$ *be an isotropic fBm of parameter* H*, with* ζ=-H-1*. fBm* $\mathbf{u}$ *can be constructed by means of the divergence-free fractional Laplacian wavelet series:*

$$\mathbf{u}_j(\mathbf{x}) = \sum_{s_i>0,\boldsymbol{\ell}} \epsilon'_{\boldsymbol{\ell},s_i}[(-\Delta)^{\frac{\zeta}{2}}\Phi^j_{\boldsymbol{\ell},s_i}(\mathbf{x})] + c \sum_{s_1,s_2>0,\boldsymbol{\ell}} \epsilon_{\boldsymbol{\ell},\mathbf{s}}[(-\Delta)^{\frac{\zeta}{2}}\Psi^j_{\boldsymbol{\ell},\mathbf{s}}(\mathbf{x})], \tag{2.28}$$

where we have low-frequency function coefficents $\epsilon'_{\boldsymbol{\ell},s_i}$*, and where according to proposition 2.2 wavelet coefficients* $\boldsymbol{\epsilon}_{\boldsymbol{\ell},\mathbf{s}}$ *are i.i.d zero-mean Gaussian variables.*

3. Bayesian estimation.

3.1. Likelihood models. We will consider in this paper two inverse-problems: image restoration and divergence-free optic-flow estimation. Let us introduce *likelihood* models. Minus their logarithms correspond to so-called data-terms noted $\mathcal{J}_l$, which give a relation between observations and the variable of interest. Let y comprise either the observed image $\{y_0\}$ to be enhanced or the image pair $\{y_0, y_1\}$ used for optic-flow estimation. In their simplest form, the restoration data-term writes:

$$\mathcal{J}_l(\boldsymbol{u}, y) = \frac{1}{2}\int_{\mathbb{R}^2} (\boldsymbol{u}(\mathbf{x}) - y_0(\mathbf{x}))^2 d\mathbf{x}, \quad \boldsymbol{u} \in L^2(\mathbb{R}^2), \tag{3.1}$$

and, for optic-flow estimation, the Displaced Frame Difference (DFD) data-term is defined as:

$$\mathcal{J}_l(\boldsymbol{u}, y) = \frac{1}{2}\int_{\mathbb{R}^2} \left(y_1(\mathbf{x} + \boldsymbol{u}(\mathbf{x})\delta t) - y_0(\mathbf{x})\right)^2 d\mathbf{x}, \quad \boldsymbol{u} \in (L^2(\mathbb{R}^2))^2 \tag{3.2}$$

In order to simplify notations we will consider in the following the case $\delta t = 1$. The maximum likelihood estimate can be defined as the functional minimum, *i.e.*, $\arg\min_{\boldsymbol{u}} \mathcal{J}_l(\boldsymbol{u}, y)$, subject to the divergence-free constraints $\mathrm{div}_{\mathbf{x}}\boldsymbol{u}(\mathbf{x}) = 0,\ \forall \mathbf{x} \in \mathbb{R}^2$ in the optic-flow case. However, it is well-known that both problems are ill-posed and need to be regularized.

3.2. Prior models . Using (2.21), simple regularization models follows from decomposition (2.28): an isotropic divergence-free fBm prior can simply be formalized by independent, identically distributed, zero-mean and normalized Gaussian distributions for fractional wavelet coefficients:

$$\begin{aligned} &\mathbf{u}_j(\mathbf{x}) = \sum_{s_i>0,\boldsymbol{\ell}} \epsilon'_{\boldsymbol{\ell},s_i}[(-\Delta)^{\frac{\zeta}{2}}\Phi^j_{\boldsymbol{\ell},s_i}(\mathbf{x})] + c \sum_{s_1,s_2>0,\boldsymbol{\ell}} \epsilon_{\boldsymbol{\ell},\mathbf{s}}[(-\Delta)^{\frac{\zeta}{2}}\Psi^j_{\boldsymbol{\ell},\mathbf{s}}(\mathbf{x})], \\ &\Lambda\boldsymbol{\epsilon} \sim \mathcal{N}(0, \Lambda), \end{aligned} \tag{3.3}$$

where $\boldsymbol{\epsilon}$ denotes a vector composed by the set of coefficients $\{\epsilon_{\boldsymbol{\ell},\mathbf{s}}, \epsilon'_{\boldsymbol{\ell},\mathbf{s}}\}$ and Λ is a diagonal matrix with unitary entries for coefficients $\epsilon_{\boldsymbol{\ell},\mathbf{s}}$ whose scale ℓ are related to the spectral range Υ, and with zero entries otherwhere. The zero entries on the diagonal of Λ implies that the multivariate Gaussian prior has an infinite variance in these directions. Note that the probabilistic model (3.3) implies the power-law decay of power spectrum $E(\kappa) \propto \kappa^{-2H-1}$, $\forall \kappa \in \Upsilon$.

3.3. Posterior estimation. The computation of unknown $\boldsymbol{u}$ is now reduced to the estimation of its fractional divergence-free wavelet coefficients, knowing that a subset of the coefficients $\epsilon_{\boldsymbol{\ell},\mathbf{s}}$ are realization of independent one-dimensional reduced and zero-mean normal distributions.

3.3.1. MAP estimate. An interesting estimate may be obtain solving the minimization problem:

$$\boldsymbol{\epsilon}^* = \arg\min_{\boldsymbol{\epsilon}} \mathcal{J}_l(\boldsymbol{\epsilon}, y), \text{ where } \Lambda\boldsymbol{\epsilon} \sim \mathcal{N}(0, \Lambda) \tag{3.4}$$

with

$$\mathcal{J}_l(\boldsymbol{\epsilon}, y) = \frac{1}{2}\int_{\mathbb{R}^2} \left(g \circ z_{\boldsymbol{\epsilon}}(\mathbf{x}) - y_0(\mathbf{x})\right)^2 d\mathbf{x},$$

where in the case of an optic-flow problem we define $(z_{\boldsymbol{\epsilon}}(\mathbf{x}) - \mathbf{x}) \in \mathcal{H}^{\zeta}_{div}(\mathbb{R}^2)$:

$$z_{\boldsymbol{\epsilon}}(\mathbf{x}) = \mathbf{x} + \sum_{s_i>0,\boldsymbol{\ell}} \epsilon'_{\boldsymbol{\ell},s_i}[(-\Delta)^{\frac{\zeta}{2}}\Phi^j_{\boldsymbol{\ell},s_i}(\mathbf{x})] + c\sum_{s_1,s_2>0,\boldsymbol{\ell}} \epsilon_{\boldsymbol{\ell},\mathbf{s}}[(-\Delta)^{\frac{\zeta}{2}}\Psi_{\boldsymbol{\ell},\mathbf{s}}(\mathbf{x})]$$

with $g(\mathbf{x}) = y_1(\mathbf{x})$, or in the case of an image restoration problem $z_{\boldsymbol{\epsilon}} \in \mathcal{H}^{\zeta}(\mathbb{R}^2)$:

$$z_{\boldsymbol{\epsilon}} : (\mathbf{x}) \to \sum_{s_i>0,\boldsymbol{\ell}} \epsilon'_{\boldsymbol{\ell},s_i}[(-\Delta)^{\frac{\zeta}{2}}\chi^j_{\boldsymbol{\ell},s_i}(\mathbf{x})] + c\sum_{s_1,s_2>0,\boldsymbol{\ell}} \epsilon_{\boldsymbol{\ell},\mathbf{s}}[(-\Delta)^{\frac{\zeta}{2}}\chi_{\boldsymbol{\ell},\mathbf{s}}(\mathbf{x})]$$

with the identity function $g(\mathbf{x}) = \mathbf{x}$. From a Bayesian perspective, (3.4) corresponds to the following Maximum A Posteriori (MAP) problem:

$$\begin{aligned} \boldsymbol{\epsilon}^* =& \arg\max_{\boldsymbol{\epsilon}} p(y|\boldsymbol{\epsilon})p(\boldsymbol{\epsilon}) \\ \text{where } p(y|\boldsymbol{\epsilon}) =& \frac{1}{Z_{y|\boldsymbol{\epsilon}}} \exp^{-\beta\mathcal{J}_l(\boldsymbol{\epsilon},y)}, \;\; p(\boldsymbol{\epsilon}) = \frac{1}{Z_{\boldsymbol{\epsilon}}} \exp^{-\frac{1}{2}\boldsymbol{\epsilon}^T\Lambda\boldsymbol{\epsilon}} \end{aligned} \tag{3.5}$$

with parameter $\beta \in \mathbb{R}^{+*}$, and where $Z_{y|\boldsymbol{\epsilon}}$ (resp. $Z_{\boldsymbol{\epsilon}}$) denote the partition function (independent of $\boldsymbol{\epsilon}$) of the likelihood $p(y|\boldsymbol{\epsilon})$ (resp. of the centered, of identical variance and uncorrelated Gaussian prior $p(\boldsymbol{\epsilon})$) distribution.

3.3.2. Regularized functional. The solution of (3.5) can simply be obtained by minimizing minus the logarithm of the posterior distribution:

$$p(\boldsymbol{\epsilon}|y) \propto p(y|\boldsymbol{\epsilon})p(\boldsymbol{\epsilon}),$$

yielding the MAP estimate:

$$\boldsymbol{\epsilon}^* = \arg\min_{\boldsymbol{\epsilon}}\{\beta\mathcal{J}_l(\boldsymbol{\epsilon}, y) + \mathcal{J}_p(\boldsymbol{\epsilon})\} \tag{3.6}$$

where $\mathcal{J}_p$, so-called regularization term, is defined as minus the logarithm of the prior, *i.e.*,

$$\mathcal{J}_p(\boldsymbol{\epsilon}) = \frac{1}{2}\boldsymbol{\epsilon}^T\Lambda\boldsymbol{\epsilon}. \tag{3.7}$$

Note that by a change of variable, (3.5) is solved equivalently by minimization with respect to independent and identically distributed Gaussian variables $c\boldsymbol{\epsilon}$ of constant variance $\frac{1}{\beta c^2}$.

3.3.3. On equivalence with other regularizers. The following proposition clarifies the equivalence of the regularizer (3.7) with the model proposed very recently in [31]. Furthermore, it shows that a particular case of (3.7) is the vorticity derivative penalization, which constitutes a popular approach in the context of fluid flow estimation [7, 33]. Let the operator $\mathbf{curl}^\dagger$ denote the formal adjoint of the scalar **curl** operator. It is given for any vectorial function $\boldsymbol{v} = (\boldsymbol{v}_1, \boldsymbol{v}_2)^t \in (L^2(\mathbb{R}^2))^2$, by the vectorial product: $\mathbf{curl}^\dagger \boldsymbol{v} = (\partial_{\mathbf{x}_1} \boldsymbol{v}_2 - \partial_{\mathbf{x}_2} \boldsymbol{v}_1)$. The scalar quantity $\mathbf{curl}^\dagger \boldsymbol{v}$ is called in the following the vorticity of the vector field $\boldsymbol{v}$.

PROPOSITION 3.1. *Let $\boldsymbol{u} \in \mathcal{H}^{\zeta}_{div}(\mathbb{R}^2)$. For an identity matrix Λ, regularization with (3.7) is equivalent to penalization of the L^2 norm of the signal fractional Laplacian derivative:*

$$\mathcal{J}_p(\boldsymbol{\epsilon}) = \frac{1}{2} \|(-\Delta)^{-\frac{\zeta}{2}} \boldsymbol{u}\|^2 \tag{3.8}$$

In the particular case $\zeta = -4$, we have:

$$\mathcal{J}_p(\boldsymbol{\epsilon}) = \frac{1}{2} \|\nabla \mathbf{curl}^\dagger \boldsymbol{u}\|^2 = \|\Delta(\boldsymbol{u})\|^2. \tag{3.9}$$

A consequence of this proposition is that, in two-dimension, an appropriate regularization for an isotropic divergence-free (resp. scalar) fBm of parameter $H = 2$ (resp. $H = 1$) is the penalization of the L^2 norm of the vorticity gradient (resp. of the Laplacian).

Proof. We have:

$$\begin{aligned}
\|(-\Delta)^{-\frac{\zeta}{2}} \mathbf{u}\|^2 &\triangleq \int_{\mathbb{R}^2} \sum_j |(-\Delta)^{-\frac{\zeta}{2}} \mathbf{u}_j(\mathbf{x})|^2 d\mathbf{x} \\
&= \int_{\mathbb{R}^2} \sum_j |\sum_{\boldsymbol{\ell},\, \mathbf{s} \,\in\, \mathrm{Z}^2} \langle \mathbf{u} / (-\Delta)^{\frac{\zeta}{2}} \tilde{\Psi}_{\boldsymbol{\ell},\mathbf{s}} \rangle (-\Delta)^{-\frac{\zeta}{2}} \Psi^j_{\boldsymbol{\ell},\mathbf{s}}(\mathbf{x})|^2 d\mathbf{x} \\
&= \sum_{\boldsymbol{\ell},\, \mathbf{s} \,\in\, \mathrm{Z}^2} \langle \mathbf{u} / (-\Delta)^{\frac{\zeta}{2}} \tilde{\Psi}_{\boldsymbol{\ell},\mathbf{s}} \rangle^2 \triangleq \boldsymbol{\epsilon}^T \boldsymbol{\epsilon},
\end{aligned}$$

which proves (3.8) and the equivalence with the regularizers proposed in [31]. Now, let us highlight the fact that penalization of the L^2 norm of the Laplacian or of the vorticity gradient are equivalent in the two-dimensional divergence-free case. Indeed, let χ be a stream function such as:

$$\mathbf{u} = \mathbf{curl}\ \chi. \tag{3.10}$$

From the definition of vorticity in 2D, one can prove that:

$$-\Delta\chi = \mathbf{curl}^\dagger\ (\mathbf{u}), \tag{3.11}$$

which implies that:

$$\|\nabla \mathbf{curl}^\dagger\ (\mathbf{u})\|^2 = \| - \nabla\Delta\chi\|^2 = \|\Delta(\mathbf{curl}\ \chi)\|^2 = \|\Delta(\mathbf{u})\|^2. \tag{3.12}$$

□

4. Optimization. Optimization strategies analogous to the algorithm proposed by [9] are used to solve the minimization problem (3.6). Optimization relies on a wavelet multi-resolution analysis based at each level on a LBFGS procedure, *i.e.*, on a quasi-Newton gradient descent algorithm subject to the strong Wolf conditions [26]. The regularization term is quadratic. Thus, in theory, for Gaussian *likelihood* models such as (3.1), the algorithm converges to the global minimum, while for non-Gaussian models such as (3.2), it is only insured to converge to the nearest local minima. Interesting wavelet-based multiresolution strategies dealing with these non-linearities have been recently proposed in [9]. The gradient descent optimization requires at each step the evaluation of the functional to be minimized and of its gradient.

We hereafter propose two alternative optimization strategies, which either imply spectral or spatial computation. The spectral optimization method, relying on an exact fractional Laplacian, is efficient for low order fractional derivatives. However in practice, for high order derivatives (typically for $\zeta > -1$), fractional wavelet bases become poorly conditioned, resulting in inefficient optimization algorithms. Nevertheless, we propose for such situations (typically for $\zeta < -1$) an efficient spatial optimization method, relying on a fractional Laplacian approximation. For the clarity of the presentation, we will restrict in the following to optic-flow functionals although it is easy to derive analogous expressions in the case of image restoration problems.

4.1. Spectral optimization method.

4.1.1. Functional analytical gradient. The following proposition proves that the functional gradient can simply be obtained by Fast Wavelet Transform (FWT).

PROPOSITION 4.1. *The gradient with respect to vector $\boldsymbol{\epsilon}$ of the functional minimized in* (3.6) *is the vector composed of wavelet coefficients, given by FWT of the two-dimensional scalar function*

$$\beta a_{\mathbf{s}} \mathbf{curl}^{\dagger}[c\,(-\Delta)^{\frac{\zeta}{2}}\,(g \circ z_{\boldsymbol{\epsilon}} - y_0)\,(\nabla_{\mathbf{x}} g) \circ z_{\boldsymbol{\epsilon}}](\mathbf{x})$$

using the orthonormal wavelet basis $\{\chi_{\boldsymbol{\ell},\mathbf{s}}, (\boldsymbol{\ell},\mathbf{s}) \in \mathbb{Z}^2\}$, supplemented by the additional vector $\Lambda\boldsymbol{\epsilon}$.

Proof. The gradient of the data-term $\mathcal{J}_l(\boldsymbol{\epsilon}, y)$ is given (in the case of the divergence-free optic-flow problem) by inner products with the fractional divergence-free wavelets:

$$\begin{aligned}
\partial_{\boldsymbol{\epsilon}_{\boldsymbol{\ell},\mathbf{s}}} \mathcal{J}_l(\boldsymbol{\epsilon}, y) &= c\langle[(g \circ z_{\boldsymbol{\epsilon}} - y_0)\,(\nabla_{\mathbf{x}} g) \circ z_{\boldsymbol{\epsilon}}](\mathbf{x}) / a_{\mathbf{s}} \mathbf{curl}[(-\Delta)^{\frac{\zeta}{2}} \chi_{\boldsymbol{\ell},\mathbf{s}}](\mathbf{x})\rangle \\
\partial_{\boldsymbol{\epsilon}'_{\boldsymbol{\ell},s_i}} \mathcal{J}_l(\boldsymbol{\epsilon}, y) &= c\langle[(g \circ z_{\boldsymbol{\epsilon}} - y_0)\,(\nabla_{\mathbf{x}} g) \circ z_{\boldsymbol{\epsilon}}](\mathbf{x}) / a_{\mathbf{s}} \mathbf{curl}[(-\Delta)^{\frac{\zeta}{2}} \chi_{\boldsymbol{\ell},s_i}](\mathbf{x})\rangle. \qquad (4.1)
\end{aligned}$$

Using Parseval's theorem we get:

$$\begin{aligned}
\partial_{\boldsymbol{\epsilon}_{\boldsymbol{\ell},\mathbf{s}}} \mathcal{J}_l(\boldsymbol{\epsilon}, y) &= c\langle[\widehat{(g \circ z_{\boldsymbol{\epsilon}} - y_0)\,(\nabla_{\mathbf{x}} g)} \circ z_{\boldsymbol{\epsilon}}](\mathbf{k}) / a_{\mathbf{s}} i(\mathbf{k}_2, -\mathbf{k}_1)^t |\mathbf{k}|^{\zeta} \hat{\chi}_{\boldsymbol{\ell},\mathbf{s}}(\mathbf{k})]\rangle \\
&= c\langle|\mathbf{k}|^{\zeta} a_{\mathbf{s}} i(-\mathbf{k}_2, \mathbf{k}_1)[\widehat{(g \circ z_{\boldsymbol{\epsilon}} - y_0)\,(\nabla_{\mathbf{x}} g)} \circ z_{\boldsymbol{\epsilon}}](\mathbf{k}), \hat{\chi}_{\boldsymbol{\ell},\mathbf{s}}](\mathbf{k})\rangle \\
&= c\langle a_{\mathbf{s}} \mathbf{curl}^{\dagger}[(-\Delta)^{\frac{\zeta}{2}}\,(g \circ z_{\boldsymbol{\epsilon}} - y_0)\,(\nabla_{\mathbf{x}} g) \circ z_{\boldsymbol{\epsilon}}](\mathbf{x}), \chi_{\boldsymbol{\ell},\mathbf{s}}](\mathbf{x})\rangle. \qquad (4.2)
\end{aligned}$$

The second inner product of (4.1) can be computed analogously. Moreover, it is straightforward to show that the gradient of the regularization term is simply:

$$\partial_{\boldsymbol{\epsilon}} \mathcal{J}_p(\boldsymbol{\epsilon}) = \Lambda\boldsymbol{\epsilon}. \qquad (4.3)$$

□

4.1.2. Spectral domain computation. Based on (4.2), we derive a spectral method for the computation of the gradient of functional minimized in (3.6). It is based on Fast Fourier Transform (FFT) and FWT:

ALGORITHM 1. **(functional gradient)**

i) FFT of the components of $[(g \circ z_{\boldsymbol{\epsilon}} - y_0)\,(\nabla_{\mathbf{x}} g) \circ z_{\boldsymbol{\epsilon}}](\mathbf{x})$,

ii) compute in Fourier domain the fractional differentiation and apply the $\mathbf{curl}^\dagger$ *operator on* $\widehat{[(g \circ z_{\boldsymbol{\epsilon}} - y_0)\,(\nabla_{\mathbf{x}} g) \circ z_{\boldsymbol{\epsilon}}]}(\mathbf{k})$

iii) inverse FFT to get $\mathbf{curl}^\dagger[(-\Delta)^{\frac{\zeta}{2}}\,(g \circ z_{\boldsymbol{\epsilon}} - y_0)\,(\nabla_{\mathbf{x}} g) \circ z_{\boldsymbol{\epsilon}}](\mathbf{x})$

iv) decompose the result by FWT using the orthogonal wavelets $a_{\mathbf{s}}\chi_{\boldsymbol{\ell},\mathbf{s}}$ *and the scaling functions* $\chi^0_{\boldsymbol{\ell},s_i}/\sqrt{2}$ *to obtain the data-term gradient* (4.2),

v) functional gradient obtained by adding vector (4.3)

In order to evaluate the functional or its gradient, one needs to reconstruct the unknown $\boldsymbol{u}$ appearing in $g \circ z_{\boldsymbol{\epsilon}}$ or $(\nabla_{\mathbf{x}} g) \circ z_{\boldsymbol{\epsilon}}$ from the fractional divergence-free wavelet coefficients $\boldsymbol{\epsilon}$. This can be done by spectral computation. Indeed, (2.28) can be rewritten as:

$$\boldsymbol{u} = \frac{1}{(2\pi)^2} \int_{(\mathbb{R}^2)^2} (d\mathbf{k}, d\mathbf{k})^T e^{i\boldsymbol{k}\cdot\mathbf{x}} i(\mathbf{k}_2, -\mathbf{k}_1)^T |\mathbf{k}|^\zeta \tag{4.4}$$
$$\int_{\mathbb{R}^2} d\mathbf{x}\Big(\sum_{s_i>0,\boldsymbol{\ell}} \frac{\epsilon'_{\boldsymbol{\ell},s_i}}{\sqrt{2}} \chi^0_{\boldsymbol{\ell},\mathbf{s}} + c \sum_{s_1,s_2>0,\boldsymbol{\ell}} \epsilon_{\boldsymbol{\ell},\mathbf{s}} a_{\mathbf{s}} \chi_{\boldsymbol{\ell},\mathbf{s}}\Big) e^{-i\boldsymbol{k}\cdot\mathbf{x}},$$

yielding the following reconstruction algorithm:

ALGORITHM 2. **(reconstruction of fBm)**

i) inverse FWT of $\boldsymbol{\epsilon}$ *using the orthogonal wavelets* $a_{\mathbf{s}}\chi_{\boldsymbol{\ell},\mathbf{s}}$ *and scaling functions* $\frac{1}{\sqrt{2}}\chi^0_{\boldsymbol{\ell},\mathbf{s}}$,

ii) FFT of this scalar function

iii) fractional differentiation and **curl** *operator in Fourier domain,*

iv) inverse FFT of the components to obtain $\boldsymbol{u}$

Algorithms 1 and 2 yield the ingredients necessary to approach the MAP estimate $\boldsymbol{\epsilon}^*$ with a gradient descent method.

4.2. Spatial optimization method. In order to avoid spectral computation of fractional differentiation, *i.e.*, preserve the low-order complexity, and by the same way, prevent numerical instabilities for large negative decay ζ, we choose to rotate the posterior in a standard divergence-free wavelet basis.

4.2.1. Rotation of the posterior. Let $\boldsymbol{d}$ denotes the set of divergence-free wavelet coefficients $\{d_{\boldsymbol{\ell},\mathbf{s}} = \langle \boldsymbol{u}/\tilde{\Psi}_{\boldsymbol{\ell},\mathbf{s}}\rangle = a_{\mathbf{s}}^{-1}\langle \chi, \chi_{\boldsymbol{\ell},\mathbf{s}}\rangle; (\boldsymbol{\ell},\mathbf{s}) \in \mathrm{Z}^2\}$. With these notations, the reconstruction formula (2.16) becomes for the vector field $\boldsymbol{u}$ and its potential χ:

$$\boldsymbol{u} = \sum_{\boldsymbol{\ell},\ \mathbf{s}\ \in\ \mathrm{Z}^2} d_{\boldsymbol{\ell},\mathbf{s}} \Psi_{\boldsymbol{\ell},\mathbf{s}}(\mathbf{x});\ \chi = \sum_{\boldsymbol{\ell},\ \mathbf{s}\ \in\ \mathrm{Z}^2} d_{\boldsymbol{\ell},\mathbf{s}} a_{\mathbf{s}} \chi_{\boldsymbol{\ell},\mathbf{s}}(\mathbf{x}). \tag{4.5}$$

The MAP estimation problem (3.6) is therefore rewritten as a minimization problem with respect to wavelet coefficients $\boldsymbol{d}$:

$$\boldsymbol{d}^* = \arg\min_{\boldsymbol{d}} \{\beta \mathcal{J}_l(\boldsymbol{d}, y) + \mathcal{J}_p(\boldsymbol{d})\} \tag{4.6}$$

$$\text{with} \quad \mathcal{J}_p(\boldsymbol{d}) = \frac{1}{2}\boldsymbol{\epsilon}(\boldsymbol{d})^T \Lambda \boldsymbol{\epsilon}(\boldsymbol{d}), \tag{4.7}$$

Therefore, fractional divergence-free wavelet coefficients $\boldsymbol{\epsilon}$ need to be expressed in terms of standard divergence-free wavelet coefficients $\boldsymbol{d}$.

PROPOSITION 4.2. *Let* $\mathbf{R}^{(\alpha)} = [r^{(\alpha)}_{\ell',\mathbf{s}',\boldsymbol{\ell},\mathbf{s}}]$, $\alpha \in \mathbb{R}/\mathbb{Z}_-$ *denote the matrix of mono-dimensional fractional Laplacian wavelet connection coefficients*

$$r^{(\alpha)}_{\ell',\mathbf{s}',\boldsymbol{\ell},\mathbf{s}} = \langle \psi_{\ell',\mathbf{s}'}, \left(\frac{-\partial^2}{\partial x^2}\right)^{\alpha} \psi_{\boldsymbol{\ell},\mathbf{s}} \rangle$$

composed at line indices $(\ell', \mathbf{s}')$ *and column indices* $(\boldsymbol{\ell}, \mathbf{s})$ *by the elements* $r^{(\alpha)}_{\ell',\mathbf{s}',\boldsymbol{\ell},\mathbf{s}}$. *Two-dimensional divergence-free fractional Laplacian wavelet coefficients are approached by a linear combination of divergence-free wavelet coefficients, implying low-dimensional matrices products :*

$$[\boldsymbol{\epsilon}] = \sum_{i=0}^{i_m} \binom{-\alpha}{i} \mathbf{R}^{(-\alpha-i)^T} \left[\boldsymbol{d}_{a_{\mathbf{s}}^{-1}}\right] \mathbf{R}^{(i)}, \ i_m \in \mathbb{N}^* \tag{4.8}$$

where $[\boldsymbol{\epsilon}]$ *and* $[\boldsymbol{d}_{\gamma_{\mathbf{s}}}]$ *represent respectively the matrix of two-dimensional fractional coefficients and two-dimensional standard coefficients* $d_{\boldsymbol{\ell},\mathbf{s}}$ *multiplied by factor* $\gamma_{\mathbf{s}}$.

Proof. Since the potential χ and fBm $\boldsymbol{u}$ have the same wavelet decomposition coefficients up to the factor $a_{\mathbf{s}}$, we can write that:

$$\epsilon_{\boldsymbol{\ell},\mathbf{s}} = \langle \mathbf{u}/(-\widetilde{\Delta})^{\frac{\zeta}{2}} \Psi_{\boldsymbol{\ell},\mathbf{s}} \rangle = a_{\mathbf{s}}^{-1} \sum_{\ell',\mathbf{s}'} d_{\ell',\mathbf{s}'} \langle \chi_{\ell',\mathbf{s}'}, (-\widetilde{\Delta})^{\frac{\zeta}{2}} \chi_{\boldsymbol{\ell},\mathbf{s}} \rangle \tag{4.9}$$

where $(-\widetilde{\Delta})^{\frac{\zeta}{2}} \chi_{\boldsymbol{\ell},\mathbf{s}}$ denotes one dual component of the fractional scalar wavelet basis. Although operator $(-\widetilde{\Delta})^{\frac{\zeta}{2}}$ is not separable, bi-dimensional connection coefficients appearing in (4.9) can be approached by generalized Newton's binomial expansion[5]:

$$\langle \chi_{\ell',\mathbf{s}'}, (-\widetilde{\Delta})^{\frac{\zeta}{2}} \chi_{\boldsymbol{\ell},\mathbf{s}} \rangle = \sum_{i=0}^{\infty} \binom{\frac{-\zeta}{2}}{i} r^{(-\frac{\zeta}{2}-i)}_{\boldsymbol{\ell'_1},\mathbf{s'_1},\boldsymbol{\ell_1},\mathbf{s_1}} r^{(i)}_{\boldsymbol{\ell'_2},\mathbf{s'_2},\boldsymbol{\ell_2},\mathbf{s_2}} \tag{4.10}$$

with the mono-dimensional connection coefficients:

$$r^{(-\frac{\zeta}{2}-i)}_{\boldsymbol{\ell'_1},\mathbf{s'_1},\boldsymbol{\ell_1},\mathbf{s_1}} = \langle \psi_{\boldsymbol{\ell'_1},\mathbf{s'_1}}, \left(\frac{-\partial^2}{\partial x^2}\right)^{-\frac{\zeta}{2}-i} \psi_{\boldsymbol{\ell_1},\mathbf{s_1}} \rangle, \tag{4.11}$$

$$r^{(i)}_{\boldsymbol{\ell'_2},\mathbf{s'_2},\boldsymbol{\ell_2},\mathbf{s_2}} = \langle \psi_{\boldsymbol{\ell'_2},\mathbf{s'_2}}, \left(\frac{-\partial^2}{\partial x^2}\right)^{i} \psi_{\boldsymbol{\ell_2},\mathbf{s_2}} \rangle. \tag{4.12}$$

[5]Generalized Newton's binomial expansion stands for any non-negative integer: $-\zeta/2 \notin \mathbb{Z}_-$. However, this is never the case since in (2.22) we have set $-\zeta/2 = H + 2$, with $H > 0$.

See appendix for details on wavelet connection coefficients computation. The infinite sum in (4.10) needs in practice to be truncated. Let us choose connection coefficients vanishing for large translation, *i.e.*, for $|\ell'_1 - \ell_1| \to \infty$ (see appendix for more details), corresponding to the following truncation order:

$$i_m = \max\{i \in \mathbb{N} | (-\zeta - 2i + 1) \in \mathbb{R}_+\}.$$

In practice, as illustrated in figures of appendix A, for sufficiently negative exponent ζ, binomial coefficients with $i > i_{max}$ weighting the expansion (4.10) are negligible, *i.e.*, the proposed truncation yields good approximations. Now, using the separable truncated expansion (4.10), (4.9) can be rewritten as low-dimensional matrices products. We have:

$$\begin{aligned} \epsilon_{\boldsymbol{\ell},\mathbf{s}} &\approx a_{\mathbf{s}}^{-1} \sum_{i=0}^{i_m} \binom{\frac{-\zeta}{2}}{i} \sum_{\boldsymbol{\ell'_1},\mathbf{s'_1}} r^{(-\frac{\zeta}{2}-i)}_{\boldsymbol{\ell'_1},\mathbf{s'_1},\boldsymbol{\ell_1},\mathbf{s_1}} \sum_{\boldsymbol{\ell'_2},\mathbf{s'_2}} d_{\boldsymbol{\ell'_1},\boldsymbol{\ell'_2},\mathbf{s'_1},\mathbf{s'_2}} r^{(i)}_{\boldsymbol{\ell'_2},\mathbf{s'_2},\boldsymbol{\ell_2},\mathbf{s_2}} \qquad (4.13) \\ [\boldsymbol{\epsilon}] &\approx \sum_{i=0}^{i_m} \binom{\frac{-\zeta}{2}}{i} \mathbf{R}^{(-\frac{\zeta}{2}-i)^T} \left[\boldsymbol{d}_{a_{\mathbf{s}}^{-1}}\right] \mathbf{R}^{(i)}. \end{aligned}$$

□

Therefore, the MAP estimation problem (4.6)-(4.7) becomes:

$$\begin{aligned} \boldsymbol{d}^* &= \arg\min_{\boldsymbol{d}} \{\beta \mathcal{J}_l(\boldsymbol{d}, y) + \mathcal{J}_p(\boldsymbol{d})\} \qquad (4.14) \\ \text{with} \quad \mathcal{J}_p(\boldsymbol{d}) &= \frac{1}{2} \|\mathbb{I}_\Lambda\{\sum_{i=0}^{i_m} \binom{\frac{-\zeta}{2}}{i} \mathbf{R}^{(-\frac{\zeta}{2}-i)^T} \left[\boldsymbol{d}_{a_{\mathbf{s}}^{-1}}\right] \mathbf{R}^{(i)}\}\|_F^2, \end{aligned}$$

where $\|A\|_F^2 = \text{trace}(A^T A)$ is the Frobenius norm of matrix A and with $\|\mathbb{I}_\Lambda\{[\boldsymbol{\epsilon}]\}\|_F^2 = \boldsymbol{\epsilon}^t \Lambda \boldsymbol{\epsilon}$.

4.2.2. Functional analytical gradient. We derive hereafter a trackable expression of the gradient of functional minimized in (4.14).

PROPOSITION 4.3. *Let us define (in the case of optic-flow problems) the functions* $z_{\boldsymbol{d}}(\mathbf{x}) - \mathbf{x} \in \mathcal{H}^\zeta_{div}(\mathbb{R}^2) : \mathbf{x} \to \sum_{\boldsymbol{\ell},\mathbf{s}} d_{\boldsymbol{\ell},\mathbf{s}} \Psi_{\boldsymbol{\ell},\mathbf{s}}(\mathbf{x})$ *and* $g(\mathbf{x}) = y_1(\mathbf{x})$. *The gradient with respect to vector* $\boldsymbol{d}$ *of the functional minimized in* (4.14) *is the vector composed of wavelet coefficients, given by FWT of the two-dimensional vectorial function*

$$\beta c \left(g \circ z_{\boldsymbol{d}} - y_0\right) (\nabla_{\mathbf{x}} g) \circ z_{\boldsymbol{d}}$$

using the dual divergence-free wavelet basis $\{\tilde{\Psi}_{\boldsymbol{\ell},\mathbf{s}}, (\boldsymbol{\ell},\mathbf{s}) \in \mathbb{Z}^2\}$, *supplemented by the additional vector whose* $(\boldsymbol{\ell},\mathbf{s})$*-th component writes*

$$\left(\sum_{i,j=0}^{i_m,j_m} \binom{\frac{-\zeta}{2}}{i} \binom{\frac{-\zeta}{2}}{j} \mathbf{R}^{(-\frac{\zeta}{2}-i)} \mathbb{I}_\Lambda\{\mathbf{R}^{(-\frac{\zeta}{2}-j)^T} \left[\boldsymbol{d}_{a_{\mathbf{s}}^{-2}}\right] \mathbf{R}^{(j)}\} \mathbf{R}^{(i)^T} \right)_{\boldsymbol{\ell},\mathbf{s}}.$$

Proof. Analogously to results in [9], it is straightforward to see that the gradient of the data-term $\mathcal{J}_l(\boldsymbol{d}, y)$ is given by inner-products with divergence-free wavelets:

$$\partial_{\boldsymbol{d}_{\boldsymbol{\ell},\mathbf{s}}} \mathcal{J}_l(\boldsymbol{d}, y) = c\langle [\left(g \circ z_{\boldsymbol{d}} - y_0\right) (\nabla_{\mathbf{x}} g) \circ z_{\boldsymbol{d}}](\mathbf{x}) / \Psi_{\boldsymbol{\ell},\mathbf{s}}(\mathbf{x}) \rangle. \qquad (4.15)$$

As a matter of fact, inner products in (4.15), *i.e.*, the data-term gradient, are simply given by a FWT of $c\left(g \circ z_{\boldsymbol{d}} - y_0\right)\left(\nabla_{\mathbf{x}} g\right) \circ z_{\boldsymbol{d}}$ using the dual basis of divergence-free wavelets. Note that an analogous expression can be obtained for image restoration defining $z_{\boldsymbol{d}} : (\mathbf{x}) \in L(\mathbb{R}^2) \rightarrow c \sum_{\boldsymbol{\ell},\mathbf{s}} d_{\boldsymbol{\ell},\mathbf{s}} \chi_{\boldsymbol{\ell},\mathbf{s}}(\mathbf{x}) \in L(\mathbb{R}^2)$. Concerning the regularization term, using the matrix equality:

$$\partial_{[\boldsymbol{d}]} \frac{1}{2} \mathbf{Trace}(\mathbf{R}^{(i)^T} [\boldsymbol{d}]^T \mathbf{R}^{(-\frac{\zeta}{2}-i)} \mathbf{R}^{(-\frac{\zeta}{2}-j)^T} [\boldsymbol{d}] \mathbf{R}^{(j)^T}) = \mathbf{R}^{(-\frac{\zeta}{2}-i)} \mathbf{R}^{(-\frac{\zeta}{2}-j)^T} [\boldsymbol{d}] \mathbf{R}^{(j)} \mathbf{R}^{(i)^T}, \tag{4.16}$$

it follows from the linearity of the trace operator that the gradient of the regularization term writes:

$$\partial_{\boldsymbol{d}_{\boldsymbol{\ell},\mathbf{s}}} \mathcal{J}_p(\boldsymbol{d}) = \sum_{i,j=0}^{i_m,j_m} \binom{\frac{-\zeta}{2}}{i} \binom{\frac{-\zeta}{2}}{j} \left(\mathbf{R}^{(-\frac{\zeta}{2}-i)} \mathbb{I}_{\Lambda} \{ \mathbf{R}^{(-\frac{\zeta}{2}-j)^T} [\boldsymbol{d}_{a_{\mathbf{s}}^{-2}}] \mathbf{R}^{(j)} \} \mathbf{R}^{(i)^T} \right)_{\boldsymbol{\ell},\mathbf{s}}, \tag{4.17}$$

where $(A)_{\boldsymbol{\ell},\mathbf{s}}$ denotes the $(\boldsymbol{\ell},\mathbf{s})$-th element of matrix A.

□

4.2.3. Spatial domain computation. Using proposition 4.3, a trackable computation of the gradient of functional minimized in (4.14) is provided by means of simple FWT and low-dimensional matrix products. Moreover, reconstruction (2.16) by inverse FWT is straightforward for any values of coefficients $\boldsymbol{d}$. We have therefore provided the two ingredients, which are necessary to approach the MAP estimate $\boldsymbol{d}^*$ with a gradient descent algorithm.

5. Experiments.

5.1. Divergence-free isotropic fBm generator. Realizations of isotropic fBm were generated using the Fourier-based reconstruction formula (4.4), yielding scalar or divergence-free vectorial fields. More precisely, in agreement with the fBm model (3.3), the wavelets coefficients $\{\epsilon_{\boldsymbol{\ell},\mathbf{s}}\}$ were sampled according to centered and reduced Gaussian white noise. Coefficents $\{\epsilon'_{\boldsymbol{\ell},\mathbf{s}}\}$, corresponding to the low frequency contribution, were neglected and arbitrarily fixed to zero. Nevertheless, in principle, they should have been drawn according to a fractional ARIMA random walk , see [24]. Isotropic fBm were then synthesized from this Gaussian white noise by application of algorithm 2.

The three following fBm realizations were synthesized in order to form an evaluation benchmark for the regularization model:

fBm-1. An isotropic fBm scalar field of 128×128 pixels, synthesized using this procedure, is displayed in figure 5.1. Pixel grey levels have been normalized. The wavelet generator was constructed from orthogonal Daubechies with 4 vanishing moments (Daubechie-4) with periodic boundary conditions. The Hurst exponent was fixed to the limit case of $H = 0$, implying in the fBm model (3.3) a fractional Laplacian wavelets $(-\Delta)^{\frac{\zeta}{2}}$ with $\zeta = -1$. Consequently, it induces in (2.23) a power spectrum behavior $E(\kappa) \propto \kappa^{-1}$ in a scale range going from the pixel size to the image dimension, *i.e.*, $\Upsilon = [1/128, 1]$. This power-law spectrum is visible in figure 5.2.

fBm-2 and fBm-3. Two divergence-free vectorial fBm fields of 128×128 for fBm-2 (resp. 256×256 for fBm-3) pixels were also synthesized using this procedure. They are displayed in figure 5.3 and figure 5.6. The wavelet generator was constructed from divergence-free biorthogonal Coiflet with 10 vanishing moments (Coiflet-10) and periodic boundary conditions. The Hurst exponent was fixed to $H = 2$ (resp. $H = 1/3$), implying in the fBm model a fractional Laplacian wavelets $(-\Delta)^{\frac{\zeta}{2}}$ with $\zeta = -3$ (resp. $\zeta = -4/3$). Consequently, it induces in (2.23) a power spectrum behavior $E(\kappa) \propto \kappa^{-5}$ (resp. $E(\kappa) \propto \kappa^{-5/3}$) in a scale range going from the pixel size to the image dimension, *i.e.*, $\Upsilon = [1/32, 1/16]$ (resp. $\Upsilon = [1/256, 1]$). This power-law spectrum is visible in figure 5.5 (resp. figure 5.8). These synthesized fields are representative of self-similar incompressible turbulent motion in the 2D and 3D case, as described by the Kolmogorov theory [20].

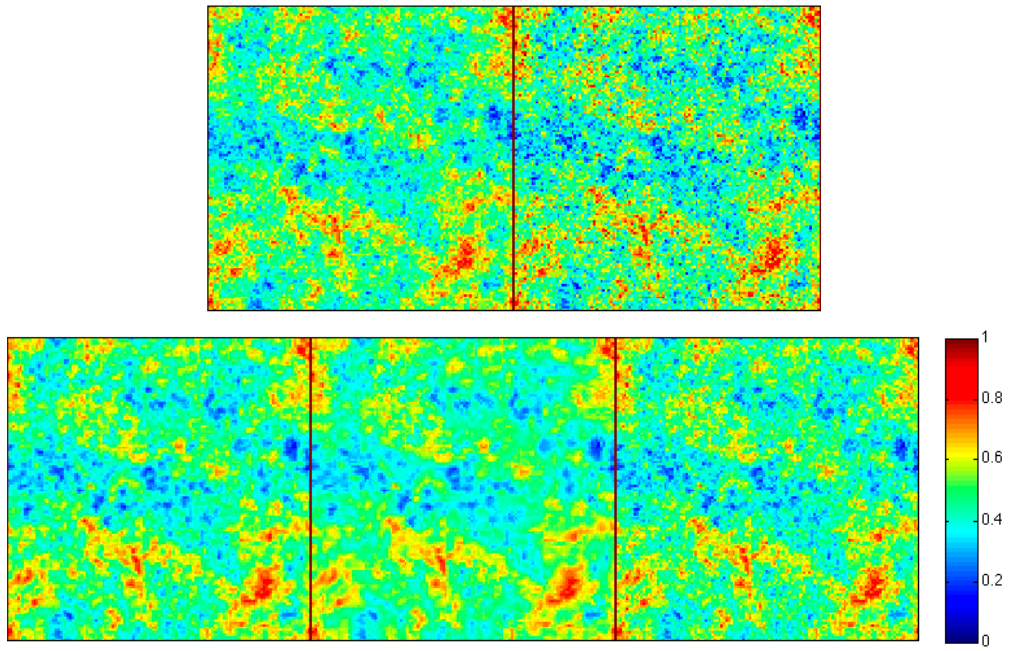

FIG. 5.1. *Above: fBm-1 realization* $\mathbf{u}(\mathbf{x})$ *(left) and observed noisy fBm-1* $y(\mathbf{x})$ *(right). Below from left to right: estimates obtain by penalizing Laplacian* L^2 *norm, using BM3D algorithm and penalizing fractional Laplacian* L^2 *norm.*

5.2. Fractal image restoration. An additive zero mean i.i.d Gaussian noise was added to the synthesized scalar field fBm-1. It resulted in a Peak Signal to Noise Ratio (PSNR) of 23.3957 dB. The scalar fBm was restored using the data-term (3.1) combined with three different regularizers/algorithms :

- *Block Matching 3D (BM3D).* This algorithm is very popular in computer vision. It has been recently proposed in [8]. It is based on nonlocal patch-wise image modeling and achieves outstanding performance in the restoration of natural scenes. The true noise variance was provided as an input to the algorithm.
- *Penalization of* L^2 *norm of Laplacian.* We used the *Matlab* implementation of this well-known deblurring algorithm. The optimal regularization parameter was chosen (using a brute-force approach).

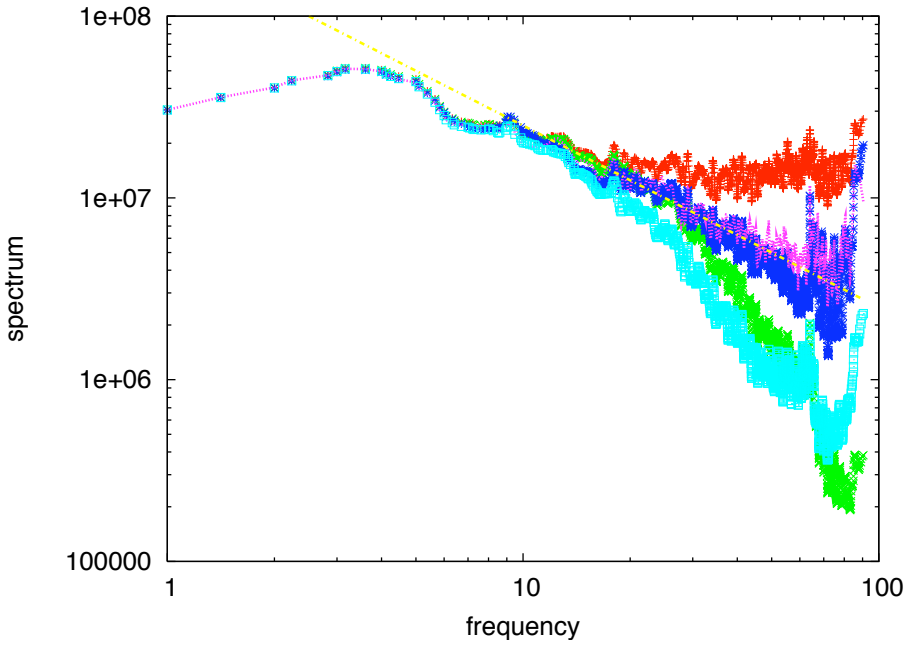

FIG. 5.2. *Power spectrum of fBm-1 with $H = 0$ (pink dashed curve), spectrum of the noisy observation (red crosses) and power law decay in $E(\kappa) \propto \kappa^{-1}$ (yellow dashed line). Estimated power spectra using BM3D algorithm (turquoise squares), Laplacian L^2 norm (green crosses) or fractional Laplacian (blue stars).*

- *Penalization of L^2 norm of fractional Laplacian* (3.8) with $\zeta = -1$. We solved (3.6) using the proposed Fourier-based optimization (see algorithm 1 and algorithm 2), since it is efficient for such a low order fractional derivative (conversely to the spatial optimization procedure, see appendix A for details). A wavelet generator identical to the one used for fBm-1 generation was employed, *i.e.*, Daubechie-4 wavelets with periodic boundary conditions.

Not surprisingly, the true prior achieved the best performances in terms of PSNR as shown in the following table.

PSNR	Obs.	BM3D	Laplacian	Frac. Laplacian
fBm.1	23.3957	26.1707	26.4211	26.4846

Moreover, as illustrated in figure 5.1, the fractional Laplacian prior succeeded to restitute the true regularity of fBm-1, while other methods seemed to fail. As shown in figure 5.2, the diagnostic is confirmed in the Fourier domain: BM3D algorithm and the Laplacian regularization over-estimate the isotropic power spectrum decay while under-estimating energy at small scales. On the contrary, the fractional Laplacian model reconstruct the true power spectrum with a good accuracy in the entire scale range.

In summary, the previous experiments highlight the fact that, efficient image restoration methods for computer vision scenes, are not necessarily adapted to fractal image restoration. An appropriate modeling is required for these irregular stochastic processes.

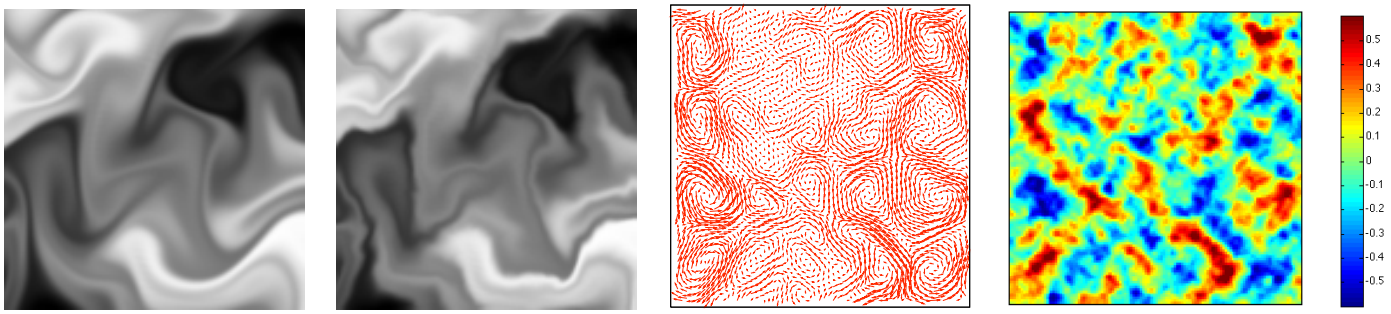

FIG. 5.3. *From left to right. Images $y_0(\mathbf{x})$ and $y_1(\mathbf{x})$, synthesized divergence-free isotropic fBm-2, vorticity of fBm-2.*

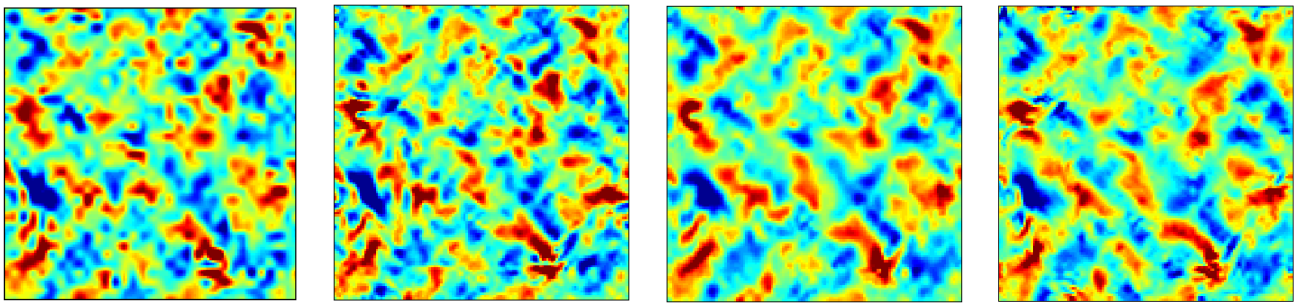

FIG. 5.4. *fBm-2 vorticity MAP estimation using (from left to right) polynomial approximation, velocity gradient penalization, vorticity gradient penalization and fractional Laplacian penalization.*

5.3. Turbulent divergence-free optic-flow estimation. Images y_1 in the data-term (3.2) were generated by deformation of an image y_0 with fBm-2 or fBm-3, *i.e.*, by the following interpolation $y_1(\mathbf{x}) = y_0(\mathbf{x} - \boldsymbol{u}(\mathbf{x}))$. We used cubic B-splines for this effect. Pixel grey levels of each of the two image couple (y_0, y_1) were then normalized. The input images y_0 and y_1 are displayed in figure 5.3 for fBm-2 (resp. figure 5.6 for fBm-3), together with their associated ground truth motion and vorticity.

The vectorial divergence-free fields fBm-2 and fBm-3 were estimated solving the minimization problem (4.6), combining the DFD data-term (3.2) with four different regularizers. Therefore, for all of these experiments, estimation was carried out in terms of coefficients of the reconstructed motion divergence-free wavelet series. The wavelet generator was constructed from divergence-free biorthogonal Coiflet-10 with periodic boundary conditions. A non negligible benefit of using wavelets is their capability to provide an efficient multiresolution analysis framework, which enables the recovery of large displacements, as shown in [9]. The four different regularization models are listed hereafter:

- *High-order polynomial approximation.* An implicit regularization by polynomial approximation is a well-known approach in computer vision. We used here local approximations by polynomials of degree 10 based on coiflet vanishing moments, as proposed in [9].
- *Penalization of L^2 norm of velocity components gradients.* The most common approach in optic-flow estimation is to penalize the velocity components gradients L^2 norm as first proposed in [17]. We used the wavelet-based implementation proposed in [19] with an optimally tuned regularization coefficient

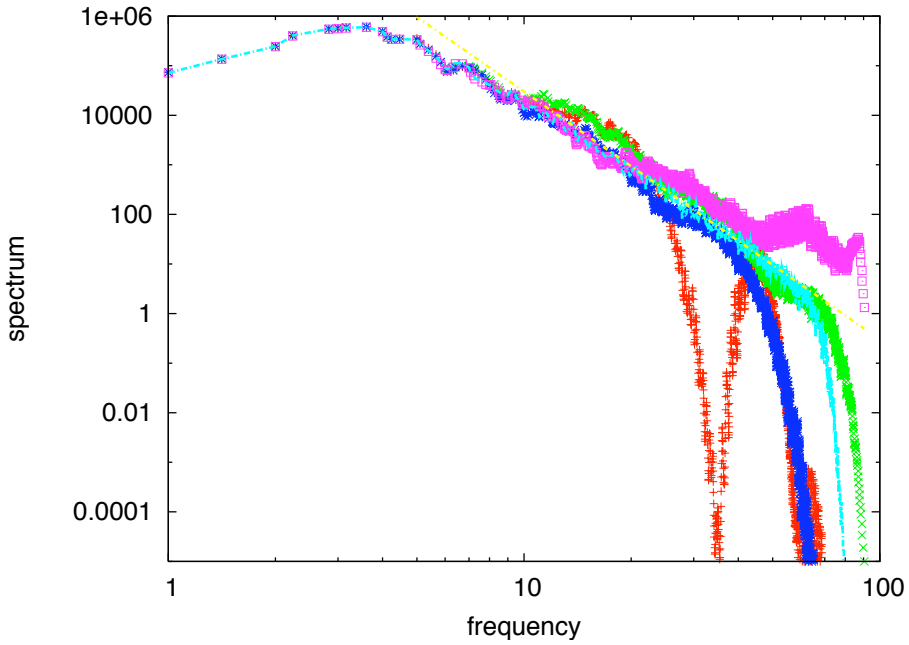

FIG. 5.5. *Power spectrum of divergence-free isotropic fBm-2 (turquoise dashed curve) and power law decay in $E(\kappa) \propto \kappa^{-5}$ (yellow dashed line). Estimated power spectra using polynomial approximation (red crosses), velocity gradient penalization (green crosses), vorticity gradient penalization (blue stars), fractional Laplacian penalization (pink squares).*

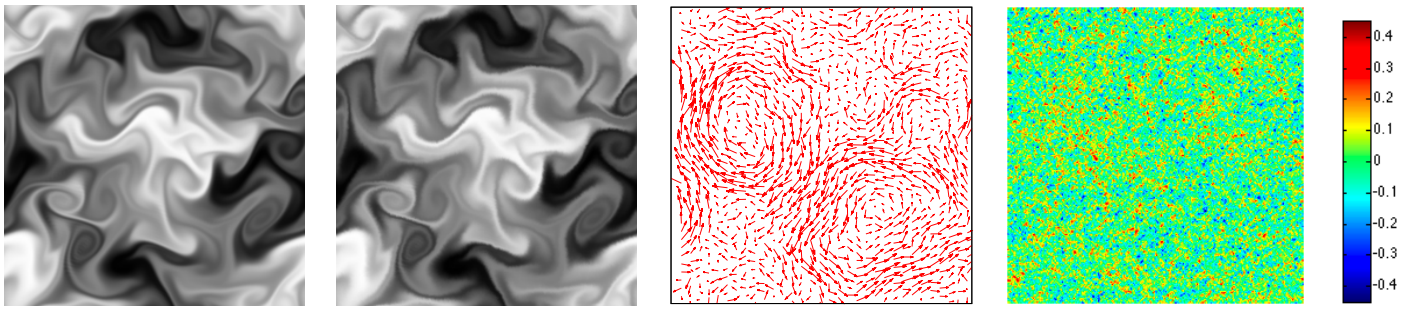

FIG. 5.6. *From left to right. Images $y_0(\mathbf{x})$ and $y_1(\mathbf{x})$, synthesized divergence-free isotropic fBm-3, vorticity of fBm-3.*

(using a brute-force approach).

- *Penalization of L^2 norm of vorticity gradient.* In fluid motion estimation a popular approach is to penalize the L^2 norm of the vorticity gradient, *i.e.*, to use model (3.9) [7, 33]. However, as remarked previously, this prior is the true regularization model for fBm only in the particular case when $H = 0$. This is not the case neither for fBm-2 nor for fBm-3. We used the wavelet-based implementation proposed in [19] with an optimally tuned regularization coefficient (using a brute-force approach).
- *Penalization of L^2 norm of fractional Laplacian* (3.8) with $\zeta = -3$ for fBm-2 (resp. $\zeta = -4/3$ for fBm-3). We used the spatial optimization method (see proposition 4.3) since it is efficient for those high order Laplacian fractional

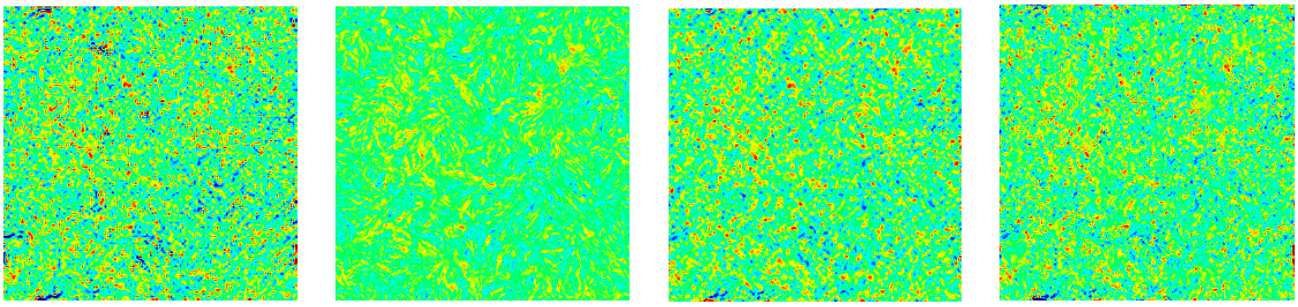

FIG. 5.7. *fBm-3 vorticity MAP estimation using (from left to right) polynomial approximation, velocity gradient penalization, vorticity gradient penalization and fractional Laplacian penalization.*

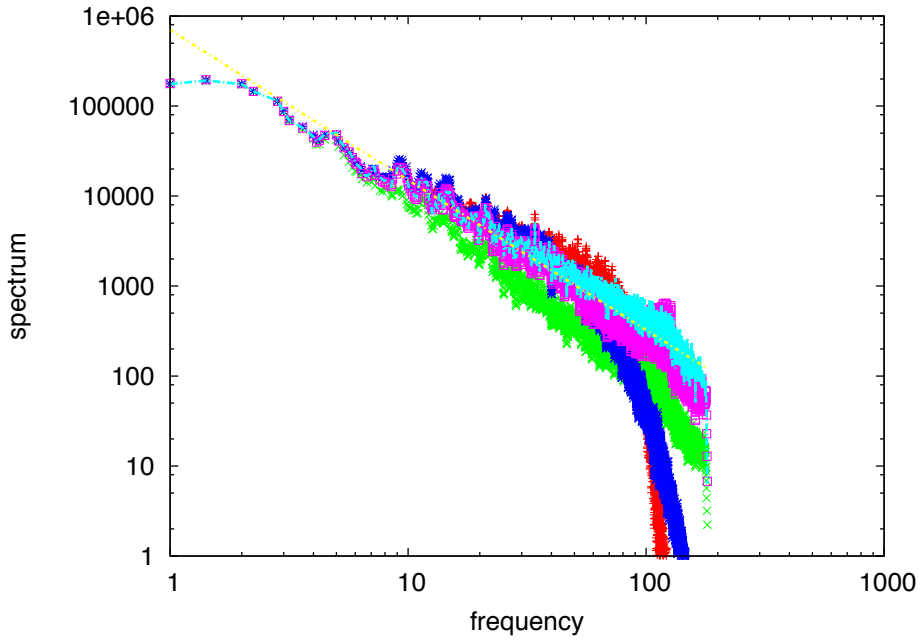

FIG. 5.8. *Power spectrum of divergence-free isotropic fBm-3 (turquoise dashed curve) and power law decay in $E(\kappa) \propto \kappa^{-5/3}$ (yellow dashed line). Estimated power spectra using polynomial approximation (red crosses), velocity gradient penalization (green crosses), vorticity gradient penalization (blue stars), fractional Laplacian penalization (pink squares).*

derivative (see appendix A for justifications).
Estimated fBm fields were evaluated based on the Root Mean Squared end-point Error (RMSE) and the Mean Barron Angular Error (MBAE), see [3]. Results are reported in the following table.

RMSE/MBAE	Polynomial	Gradient	Vorticity gradient	Frac. Laplacian.
fBm.2	0.706/19.543	0.563/14.759	0.530/14.314	0.454/11.859
fBm.3	0.213/ 7.159	0.195/7.266	0.212/7.234	0.156/5.305

Using appropriate fBm priors, that is to say fractional Laplacian regularizers, yields clearly the best results in terms of RMSE or MBAE criteria. The enhancement

in reconstruction accuracy brought by those priors is more striking than in the previous image restoration experiments. The choice of the regularization model is likely to have here a greater influence, since optic-flow estimation is not a closed problem conversely to image restoration. Consequently, if some physical knowledge about the signal is available, *e.g.*, if we know that the flow can be represented by Kolmogorov's turbulence model [20], it is crucial to design accordingly some appropriate fBm prior. We now compare and focus on vorticity fields computed from estimated motion fields. Indeed, the quality of the reconstruction of this quantity is an important matter in turbulence. Figure 5.4 (resp. figure 5.7) shows that the vorticity regularity of fBm-2 (resp. of fBm-3) is better preserved using the proposed regularization. In particular, these figures show the limitation of standard approaches: penalizing the gradient of velocity or the gradient of vorticity yields coherent vorticity blobs with smooth edges, which are not representative of fBm. As shown in figure 5.5 and figure 5.8, inspection of power spectra computed with inappropriate priors reveals an over-estimation (resp. an under-estimation) of the energy of fBm-2 (resp. of fBm-3) at intermediate scales (resp. at small scales), *i.e.*, a non respect of the spectrum power-law decay. Note that for the estimation of fBm-2, the slight deviation induced by the proposed regularization from the true spectrum at small scales has a negligible influence in terms of RMSE and MBAE since the spectrum decay is very important in this case.

6. Conclusion. In this paper we introduce a prior model for regularization of isotropic divergence-free fBm of parameter H. Realizations of these stochastic processes belong to the Sobolev function space $(\mathcal{H}^{\zeta}(\mathbb{R}^2))^2$, with ζ=-H-1 and satisfy weak divergence-free property. We show that these probabilistic models can be constructed by means of divergence-free fractional Laplacian wavelet series and prove that a subset of coefficients of the series are distributed according to Gaussian white noise. We then propose to use these prior models for regularization of ill-conditioned problems in a Bayesian framework. We point out some particular cases where the proposed model corresponds to well-known or more recent regularizers. We design two optimization strategies in order to access the MAP estimate by gradient descent algorithms. The first method relies on the computation by FFT and FWT of fractional Laplacian wavelets and is efficient for small values of H. It exploits the very simple expression of fBm prior with fractional Laplacian wavelet series. We complement this Fourier-based method by a low complexity optimization algorithm which is efficient for large values of H. It only implies FWT computation and low-dimensional matrix products. It exploits the expression of these fractional priors rotated in standard divergence-free wavelet bases by the mean of fractional Laplacian wavelet connection coefficients. We finally show weaknesses of state-of-the-art regularizers and the usefulness of these fBm prior models in the context of fractal image restoration and estimation of turbulent motion fields from image couples.

Acknowledgments. The authors would like to thank Frédéric Lavancier for his helpful comments, which have helped to improve the paper.

Appendix A. Fractional Laplacian wavelet connection coefficients.

Note that by simple bi-dimensional wavelet transform, one can derive the matrices of wavelet connection coefficients from the matrix of scaling function connection

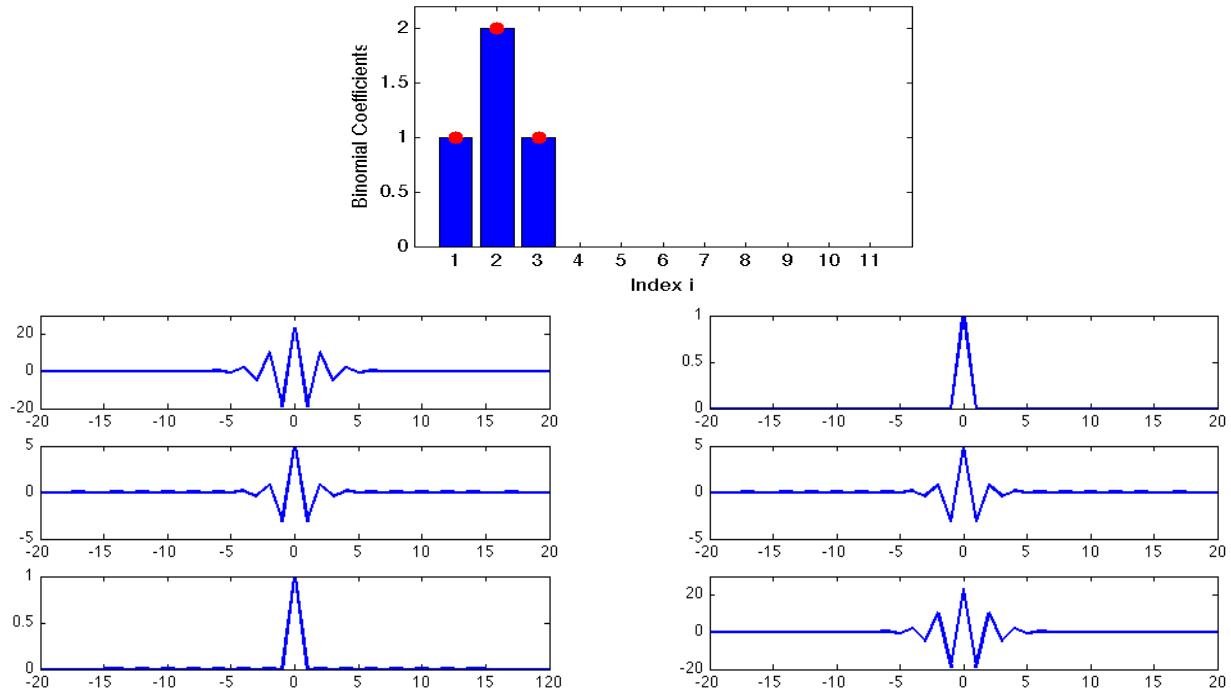

FIG. A.1. *Above: binomial coefficients in* (A.1) *for* ζ*=-4 (red dots indicate non-neglected coefficients,* i.e., $i \leq i_m$*=3). Below: connection coefficients* $r_{\ell,0}^{(-\frac{\zeta}{2}-i)}$ *(left) and* $r_{\ell,0}^{(-i)}$ *(right) in function of* ℓ*, for* $i \leq i_m$ *(from top to bottom i=1, 2 and 3).*

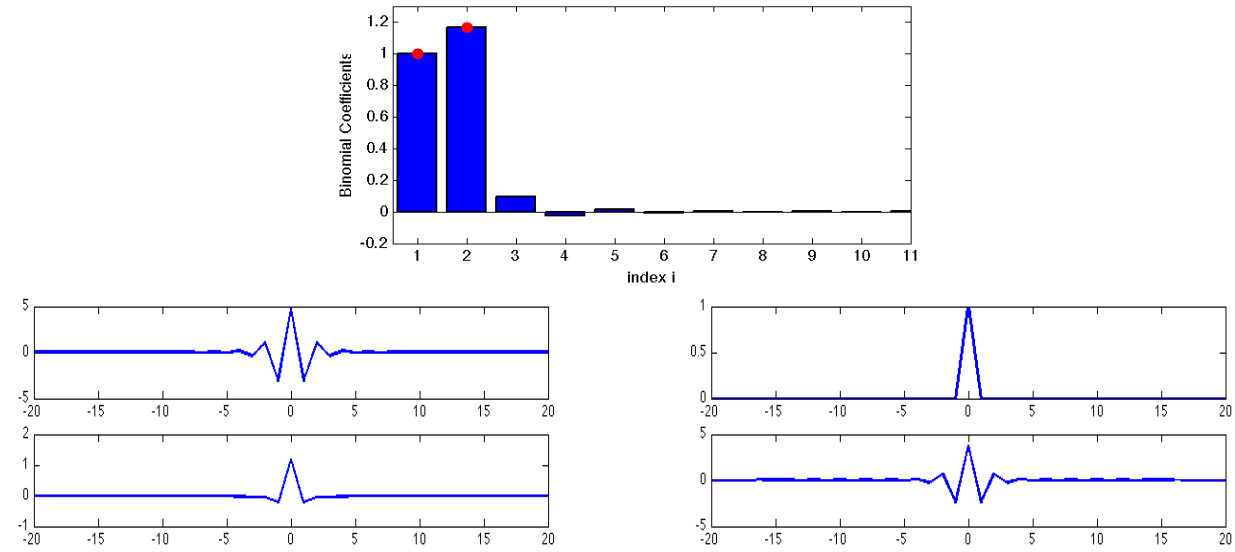

FIG. A.2. *Above: binomial coefficients in* (A.1) *for* ζ*=-7/3 (red dots indicate non-neglected coefficients,* i.e., $i \leq i_m$*=2). Below: connection coefficients* $r_{\ell,0}^{(-\frac{\zeta}{2}-i)}$ *(left) and* $r_{\ell,0}^{(-i)}$ *(right) in function of* ℓ*, for* $i \leq i_m$ *(from top to bottom i=1 and 2).*

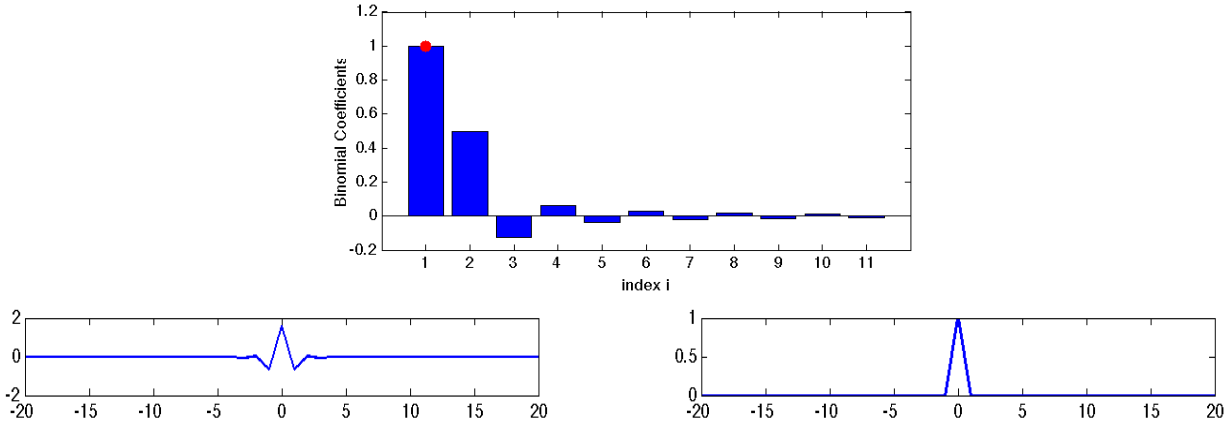

FIG. A.3. *Above: binomial coefficients in* (A.1) *for* ζ*=-1 (red dots indicate non-neglected coefficients,* i.e.*,* $i \leq i_m$*=1). Below: connection coefficients* $r_{\ell,0}^{(-\frac{\zeta}{2}-i)}$ *(left) and* $r_{\ell,0}^{(-i)}$ *(right) in function of* ℓ*, for* $i \leq i_m$ *(*$i = 1$*).*

coefficients. Indeed, (4.13) can be rewritten as:

$$[\boldsymbol{\epsilon}] = \sum_{i=0}^{i_m} \binom{\frac{-\zeta}{2}}{i} \mathbf{P}^{-1}\mathbf{R}_0^{(-\frac{\zeta}{2}-i)^T}\mathbf{P}\ [\boldsymbol{d}]\ \mathbf{P}^{-1}\mathbf{R}_0^{(i)}\mathbf{P}, \tag{A.1}$$

where $\mathbf{P}^T\mathbf{R}_0^{(\frac{\alpha}{2})}\mathbf{P}$ represents the wavelet transform of $\mathbf{R}_0^{(\frac{\alpha}{2})}$ and where $\mathbf{R}_0^{(\frac{\alpha}{2})}$ denotes a matrix whose elements are connection coefficients between standard $\varphi(x)$ and fractional Laplacian scaling functions at the finest scale:

$$r_{\ell,0}^{(\frac{\alpha}{2})} = \int_{-\infty}^{+\infty} \varphi(x-\ell) \left(\frac{-\partial^2}{\partial x^2}\right)^{\frac{\alpha}{2}} \varphi(x)dx. \tag{A.2}$$

Let us note that the truncated series (A.1) constitutes a good approximation for sufficiently large negative values of exponents ζ. Indeed as shown in figure A.1, A.2 and A.3, relation (A.1) is exact for $\zeta = -4$ or almost exact for $\zeta = -7/3$, while it constitutes a poor approximation for $\zeta = -1$. For $\alpha/2 \in \mathbb{N}$, fractional Laplacian operator becomes a standard differentiation, up to factor $(-1)^{\alpha/2}$. In order to easily compute (A.2) in a more general case, the fractional Laplacian operator is rewritten as a convolution operator. Indeed, if $(\alpha+1)/2 \in \mathbb{R}/\mathbb{N}$, fractional Laplacian can also be defined by Riesz potential[6] [15]:

$$\left(\frac{-\partial^2}{\partial x^2}\right)^{\frac{\alpha}{2}} \varphi(x) = \frac{1}{c_\alpha} \int_{-\infty}^{+\infty} \frac{\varphi(z)}{|x-z|^{\alpha+1}} dz, \tag{A.3}$$

with $c_\alpha = \frac{\sqrt{\pi}\Gamma(-\alpha/2)2^{-\alpha}}{\Gamma((1+\alpha)/2)}$. In the previous expression, the convolution kernel writes

$$k(x) = \frac{1}{c_\alpha |x|^{\alpha+1}}.$$

[6] This definition can be extend to the case $(\alpha+1)/2 \in \mathbb{N}$ using some appropriate kernel, see *e.g.*, [28]

Using the framework proposed by Beylkin, we obtain with this kernel the recursion[4][5]:

$$r_{\ell,0}^{(\frac{\alpha}{2})} = 2^{\alpha} \sum_{k=0}^{L-1} \sum_{j=k}^{k-L-1} h[k]h[k-j]r_{j+2\ell,0}^{(\frac{\alpha}{2})}, \tag{A.4}$$

subject to the asymptotics of $r_{\ell,0}^{(\frac{\alpha}{2})}$ for large translation ℓ:

$$r_{\ell,0}^{(\frac{\alpha}{2})} = \begin{cases} \dfrac{1}{c^{\alpha}\ell^{1+\alpha}} + \mathcal{O}\left(\dfrac{1}{\ell^{1+\alpha+2n}}\right) & \text{for } \ell > 0, \\ \dfrac{1}{c^{\alpha}(-\ell)^{1+\alpha}} + \mathcal{O}\left(\dfrac{1}{(-\ell)^{1+\alpha+2n}}\right) & \text{for } \ell < 0. \end{cases} \tag{A.5}$$

By a direct inversion procedure, we solve linear system (A.4), which is of infinite dimension, but where coefficients have been approached by the asymptotic laws (A.5) for sufficiently large translations. Note that, for large negative translations, the asymptotic of connection coefficients differs from the asymptotic of standard fractional differentiation coefficients of [4].

REFERENCES

[1] Abry, P., Sellan, F.: The wavelet-based synthesis for fractional brownian motion proposed by f. sellan and y. meyer: Remarks and fast implementation. Applied and Computational Harmonic Analysis **3**, 377–383 (1996)

[2] Amblard, P.O., Coeurjolly, J.F., Lavancier, F., Philippe, A.: Basic properties of the multivariate fractional Brownian motion. Rapport de recherche hal-00497639, HAL (2010)

[3] Baker, S., Scharstein, D., Lewis, J., Roth, S., Black, M., Szeliski, R.: A database and evaluation methodology for optical flow. In: Int. Conf. on Comp. Vis., ICCV 2007 (2007)

[4] Beylkin, G.: On the representation of operator in bases of compactly supported wavelets. SIAM J. Numer. Anal **6**(6), 1716–1740 (1992)

[5] Beylkin, G.: Wavelets and fast numerical algorithms. Lecture Notes for short course, AMS-93 (1993)

[6] Blu, T., Unser, M.: Self-similarity: Part ii optimal estimation of fractal processes. Signal Processing, IEEE Transactions on **55**(4), 1364 –1378 (2007)

[7] Corpetti, T., Mémin, E., Pérez, P.: Dense estimation of fluid flows. Pattern Anal Mach Intel **24**(3), 365–380 (2002)

[8] Dabov, K., Foi, A., Katkovnik, V., Egiazarian, K.: Image denoising by sparse 3-d transform-domain collaborative filtering. Image Processing, IEEE Transactions on **16**(8), 2080 –2095 (2007)

[9] Dérian, P., Héas, P., Herzet, C., Mémin, E.: Wavelet-based fluid motion estimation. In: 3rd International Conference on Scale-Space and Variational Methods in Computer Vision (SSVM2011), IEEE LNCS. Ein-Gedi, Israel (2011)

[10] Derian, P., Heas, P., Memin, E.: Wavelets to reconstruct turbulence multifractals from experimental image sequences. In: 7th Int. Symp. on Turbulence and Shear Flow Phenomena, TSFP-7. Ottawa, Canada (2011)

[11] Deriaz, E., Perrier, V.: Divergence-free and Curl-free wavelets in 2D and 3D, application to turbulence. J. of Turbulence **7**, 1–37 (2006)

[12] Elliott, F., Horntrop, D., Majda, A.: A fourier-wavelet monte carlo method for fractal random fields. Journal of Computational Physics **2**, 384–408 (1996)

[13] Flandrin, P.: On the spectrum of fractional brownian motions. Information Theory, IEEE Transactions on **35**(1), 197 –199 (1989)

[14] Flandrin, P.: Wavelet analysis and synthesis of fractional brownian motion. IEEE Trans. on Info. Theory **38(2)**(910-917) (1992)

[15] Gorenflo, R., Mainardi, F.: Random walk models for space-fractional diffusion processes. Fractional Calculus and Applied Analysis **1**(2), 167–191 (1998)

[16] Heas, P., Memin, E., Heitz, D., Mininni, P.: Power laws and inverse motion modeling: application to turbulence measurements from satellite images. Tellus A (2011)

[17] Horn, B., Schunck, B.: Determining optical flow. Artificial Intelligence **17**, 185–203 (1981)

[18] Jalobeanu, A., Zerubia, J., Blanc-Fraud, L.: Bayesian estimation of blur and noise in remote sensing imaging. In: P. Campisi, K. Egiazarian (eds.) Blind image deconvolution: theory and applications. CRC Press (2007)
[19] Kadri-Harouna, S., Derian, P., Heas, P., Memin, E.: Divergence-free wavelets and high order regularization. submitted (2011)
[20] Kolmogorov, A.: The local structure of turbulence in inompressible viscous fluid for very large reynolds number. Dolk. Akad. Nauk SSSR **30**, 301–5 (1941)
[21] Lemarié-Rieusset, P.: Analyses multirésolutions non orthogonales, commutation entre projecteurs et dérivation et ondelettes vecteurs à divergence nulle. Revista Matematica Iberoamericana **8**, 221–237 (1992)
[22] Mallat, S.: A Wavelet Tour of Signal Processing: The Sparse Way. Academic Press (2008)
[23] Mandelbrot, B.B., Ness, J.W.V.: Fractional brownian motions, fractional noises and applications. SIAM Review **10**, 422–437 (1968)
[24] Meyer, Y., Sellan, F., Taqqu, M.S.: Wavelets, generalized white noise and fractional integration: the synthesis of fractional brownian motion. J. of Fourier Analysis and Applications **5**(5), 465–494 (1999)
[25] Monin, A., Yaglom, A.: Statistical Fluid Mechanics: Mechanics of Turbulence. JDover Pubns (1971)
[26] Nocedal, J., Wright, S.J.: Numerical Optimization. Springer Series in Operations Research. Springer-Verlag, New York, NY (1999)
[27] Reed, I., Lee, P., Truong, T.: Spectral representation of fractional brownian motion in n dimensions and its properties. Information Theory, IEEE Transactions on **41**(5), 1439 –1451 (1995)
[28] Reichel, W.: Characterization of balls by riesz-potentials. Annali di Matematica Pura ed Applicata **188**, 235–245 (2009)
[29] Tafti, P., Van De Ville, D., Unser, M.: Invariances, laplacian-like wavelet bases, and the whitening of fractal processes. IEEE Transactions on Image Processing **18**(4), 689–702 (2009)
[30] Tafti, P.D., Unser, M.: Fractional Brownian vector fields. Multiscale modeling & simulation **8**(5), 1645–1670 (2010)
[31] Tafti, P.D., Unser, M.: On regularized reconstruction of vector fields. Image Processing, IEEE Transactions on **20**(11), 3163 –3178 (2011)
[32] Tirosh, S., Van De Ville, D., Unser, M.: Polyharmonic smoothing splines for multi-dimensional signals with fractal-like spectra. In: Proceedings of ICASSP., vol. 3, pp. iii – 297–300 vol.3 (2004)
[33] Yuan, J., Schnörr, C., Memin, E.: Discrete orthogonal decomposition and variational fluid flow estimation. Journ. of Math. Imaging & Vison **28**, 67–80 (2007)